J. Fluid Mech. (1982), *vol.* 116, *pp.* 157–186
Printed in Great Britain

Self-sustained low-frequency components in an impinging shear layer

By C. KNISELY† AND D. ROCKWELL

Department of Mechanical Engineering and Mechanics,
Lehigh University, Bethlehem, PA 18015

(Received 6 October 1980 and in revised form 8 June 1981)

Oscillations of a cavity shear layer, involving a downstream-travelling wave and associated vortex formation, its impingement upon the cavity corner, and upstream influence of this vortex–corner interaction are the subject of this experimental investigation.

Spectral analysis of the downstream-travelling wave reveals low-frequency components having substantial amplitudes relative to that of the fundamental (instability) frequency component; using bicoherence analysis it is shown that the lowest-frequency component can interact with the fundamental either to reinforce itself or to produce an additional (weaker) low-frequency component. In both cases, all frequency components exhibit an overall phase difference of almost $2k\pi$ ($k = 1, 2, \ldots$) between separation and impingement. Furthermore, the low-frequency and fundamental components have approximately the same amplitude growth rates and phase speeds; this suggests that the instability wave is amplitude-modulated at the low frequency, as confirmed by the form of instantaneous velocity traces.

At the downstream corner of the cavity, successive vortices, arising from the amplified instability wave, undergo organized variations in (transverse) impingement location, producing a low-frequency component(s) of corner pressure. The spectral content and instantaneous trace of this impingement pressure are consistent with those of velocity fluctuations near the (upstream) shear-layer separation edge, giving evidence of the strong upstream influence of the corner region.

1. Introduction

In recent years, self-sustained oscillations of impinging shear layers such as the jet–edge, mixing-layer–edge, and cavity-shear-layer–corner configurations have been extensively investigated with the objectives of attenuating noise generation and flow-induced vibrations of structural components. The review of Rockwell & Naudascher (1979), for example, summarizes characteristics of these oscillations. The general features of such oscillations are illustrated in figure 1 for the case of a cavity flow. Studies of this class of flows have focused on the primary (or predominant) frequency of oscillation arising from hydrodynamic instability of the separated shear layer, its variation with flow velocity and impingement length, occurrence of jumps in frequency, and possible hysteresis effects. Relatively little attention has been given

† Present address: Strömungslabor 1504, Gebrüder Sulzer A.G., CH-8401 Winterthur, Switzerland.

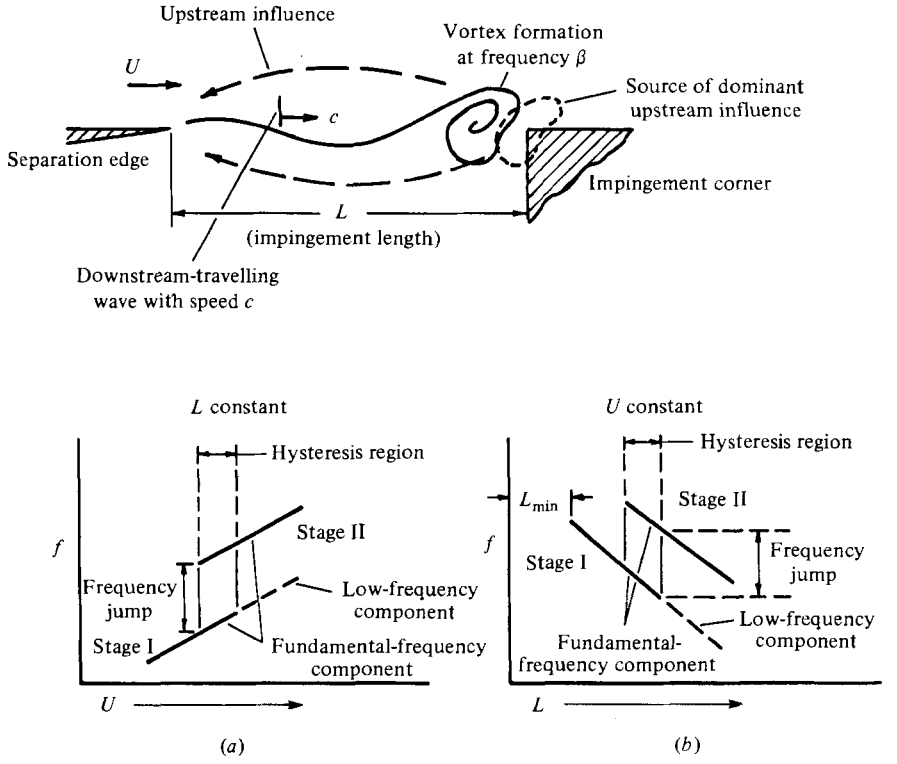

FIGURE 1. Schematics of physical mechanisms associated with oscillations of an impinging flow; and frequency variation with (*a*) varying free-stream velocity U, fixed impingement length L, and (*b*) fixed free-stream velocity, varying impingement length.

to oscillation components having frequencies *lower* than the fundamental. Yet the time-averaged spectra of velocity fluctuations in mixing-layer–edge (Hussain & Zaman 1978), cavity (Rockwell & Knisely 1979*a*, 1980*b*) and jet–edge (Stegen & Karamcheti 1970) configurations exhibit well-defined low-frequency components, thereby strongly suggesting that there is a well-defined mechanism for generating these components, common to a number of flow-structure geometries.

A thorough definition of the physical mechanism(s) generating and sustaining the low-frequency components rests upon an understanding of the cycle of events giving rise to self-sustained oscillations at the fundamental frequency of shear-layer instability; consequently, this aspect is briefly discussed here. In their review of self-sustained oscillations of impinging shear layers, Rockwell & Naudascher (1979) emphasize the following features common to a diverse group of flow configurations.

(*a*) *Feedback, or upstream influence, due to disturbances arising from unsteady flow–corner or wedge interaction at impingement* (see figure 1). For the conditions examined herein (low-speed water flow), the acoustic wavelength is much longer than the impingement length; therefore, this upstream influence is essentially instantaneous and can be described as 'pseudo-sound' (Ffowcs Williams 1969). That is, changes in concentration of vorticity (e.g. severe distension), associated with sudden changes in velocity and pressure at the impingement corner or edge, result in corresponding velocity and pressure perturbations in upstream regions of the flow, having the greatest

consequence in the highly sensitive region near shear-layer separation. Of course, even non-impinging concentrations of vorticity have an upstream influence in accordance with the Biot–Savart law. But the drastic change in flow-boundary conditions at the impingement edge is the source of dominant upstream influence; in fact, Powell (1961) has shown that unsteady-flow–edge interaction gives rise to a strong dipole source at the edge, whose dominant effect is imprinted upon the receptive region of the upstream flow near separation. Moreover, Ziada & Rockwell (1982) and Rockwell & Knisely (1979*a*, *b*) have shown that the presence of an impingement edge or corner gives strongly organized fluctuations at the upstream separation edge; without the downstream edge or corner, they are undetectable.

In the present study, this upstream influence is amplitude-modulated; it arises from ordered variations in the impingement location of vortices upon a corner, producing amplitude modulations of the pressure and velocity fluctuations in the impingement region. The upstream consequence is induction of corresponding, amplitude-modulated fluctuations in the sensitive region near separation; indeed, velocity fluctuations at separation are relatively strong, displaying time-averaged spectra and instantaneous traces that are qualitatively similar to those at impingement. These fluctuations induced at separation are, in turn, amplified in the downstream shear layer.

(*b*) *Amplification of induced disturbances in the shear layer from separation to impingement* (see figure 1). In accordance with linear (spatial) stability theory (Michalke 1965), disturbances are amplified exponentially with streamwise distance provided their amplitude remains sufficiently small; such is the case in the region immediately downstream of the separation edge. The aforementioned upstream influence arising from vortex–corner interaction provides the organized perturbations at separation that are subsequently amplified, first exponentially, then departing from this exponential (often called 'linear') growth because of finite-amplitude effects at locations farther downstream. These amplified disturbances (usually vortices) impinge upon the downstream corner, in turn producing an upstream influence, thereby closing the loop for sustaining the oscillations. The downstream-travelling wave associated with the amplifying disturbance is typically represented by an amplification factor ($-\alpha_i$) and a single wavenumber (α_r) (Michalke 1965), simplifying its analytical and experimental characterization.

In this investigation, the disturbance arriving at the upstream separation edge from the downstream corner region is amplitude-modulated; moreover, the disturbance amplified between separation and impingement maintains its amplitude-modulated character, as evidenced by instantaneous velocity traces, as well as by the growth rates $-\alpha_i$ and phase speeds c of all frequency components associated with the amplitude-modulated wave. The extent to which this growth of the modulated disturbance involves nonlinear interactions will be addressed.

The objectives of this study are to characterize the above aspects of self-sustained, amplitude modulation of impinging shear layers. Following a description of the experimental system, these points will be addressed: the overall variations of the fundamental and low-frequency components associated with amplitude modulation as a function of impingement length L and free-stream velocity U; the examination of nonlinear interaction between frequency components; the source of dominant upstream influence, i.e. vortex–corner interaction mechanisms; the nature of growth of the amplitude-modulated instability wave travelling downstream through the shear layer along the

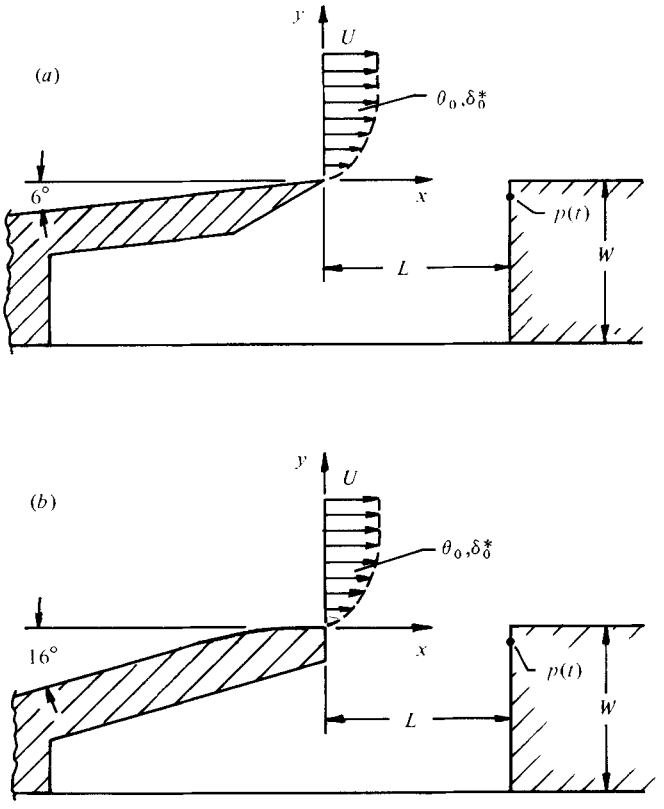

FIGURE 2. Two acceleration-ramp geometries and nomenclature.

mouth of the cavity; and, finally, overall phase conditions between separation and impingement for the fundamental and low-frequency components of the amplitude-modulated wave.

2. Experimental system and instrumentation

Experiments were carried out in a recirculating water channel having a test section 30·4 cm wide and 45·7 cm high. As described in previous studies (Rockwell & Knisely 1979*a*, *b*, 1980*a*), in order to provide a well-defined boundary layer at separation, the flow was divided into two parts, one passing beneath the rig, the other passing over the cavity. The flow passing over the cavity arrangement was accelerated before separation. Several acceleration ramp geometries were employed for initial diagnostics. To maximize the spanwise coherence of the shear layer along the mouth of the cavity, and minimize contamination by the large-scale recirculation vortex, which may, in the case of the classical rectangular cavity (Maull & East 1963; Rockwell & Knisely 1980*a*), exert three-dimensional influences, the geometries of figure 2 were employed. Extensive flow visualization of the spanwise character of the free shear layer showed a strong coherence for the range of impingement lengths and velocities examined herein. At lengths longer than those reported in this investigation, the sinuous warping of the transverse vortex core reported earlier (Konrad 1976; Breidenthal 1979; Rockwell & Knisely 1980*a*) was observed. Design of the separation edge was

stimulated by the suggestion of Morkovin & Paranjape (1971) that a sharp edge optimizes receptivity to incident disturbances. While both ramps produced well-defined oscillations having a very similar character, the oscillations associated with the ramp (*a*) were slightly stronger, and it was used in the majority of experiments. At a Reynolds number (based on θ_0, momentum thickness at separation) of 190, the two ramps produced flows with approximately equal momentum thicknesses

$$(\theta_0 = 0{\cdot}075 \pm 0{\cdot}005 \text{ cm})$$

but slightly different shape factors ($H_a = 1{\cdot}90$, $H_b = 2{\cdot}20$). The two ramps resulted in unsteady fields with velocity and pressure spectra of essentially identical character at $R_{\theta_0} = 190$ over the range of lengths of interest. Unless otherwise stated, the data presented were obtained using the ramp in figure 2(*a*).

Velocity measurements were made with DISA hot-film probes using a DISA 55D01 anemometer in conjunction with a DISA 55M25 linearizer. The impingement edge of the cavity was fitted with a pressure tap 0·24 cm below the impingement corner. A Kulite XCS-093-2D bonded strain gauge transducer was used to measure the fluctuating pressure. Both the velocity signal and the pressure signal were passed through identical Krohn-Hite Model 3700 band-pass filters and class A variable-gain (from 1 to 1000) amplifiers. The nominal filtering frequencies were two octaves above and below any frequencies of interest.

The injection of dye into the boundary layer prior to separation and into the recirculating cavity volume permitted visualization of the discrete vortical structures. The simultaneous recording of dye visualization and fluctuations in velocity and pressure was accomplished with a dual-camera, split-screen, high-speed Instar video recording system. One camera recorded the visualization while the other was focused on the screen of a dual-trace storage oscilloscope displaying the fluctuating pressure and velocity signals. The video tape was played back in slow motion/stop action and photographs were made of the screen for inclusion in this paper.

The fluctuating pressure and velocity signals were processed using a PDP-8 minicomputer to sample, digitize, and perform spectral analysis of the fluctuating signals. An alternative process, involving digital recording of the fluctuating signals on cassettes, using a Nicolet 1090A digital oscilloscope with appropriate interfaces, and then processing on a CDC 6400 computer, was employed for the estimation of cross spectra of fluctuating velocity and pressure, bispectra, and bicoherence spectra. Unless otherwise noted, power spectra presented are from the PDP-8 minicomputer.

In order to characterize fundamental and low-frequency components of the oscillation, a range of conditions, involving twofold variations in velocity and impingement length, were examined. A large number of amplitude spectra taken over these ranges provided a composite overview of the frequencies and amplitudes of the discrete oscillation components.

3. Variation of fundamental and low-frequency components with impingement length and free-stream velocity

From previous investigations (e.g. Sarohia 1975), and as shown schematically in figure 1, the fundamental frequency of shear-layer oscillation is expected to vary with both impingement length L and free-stream velocity U. In this investigation, spectra

of pressure fluctuations measured at impingement indicate the existence of well-defined subharmonics in the cavity shear layer both before and after the frequency jump (the discontinuity in the f *vs.* L and f *vs.* U plots). To determine the behaviour of possible low-frequency components, as well as to confirm that of the fundamental, two sets of pressure fluctuation spectra were recorded. In the first series of measurements, the free-stream velocity was held constant while the impingement length was varied. In the second series, the impingement length was fixed and the free-stream velocity varied. In discussing both sets of data and throughout this paper, the subscript I will be used to denote parameters in stage I prior to the frequency jump where a single subharmonic is present. The subscript II will be used to distinguish parameters associated with oscillations occurring in stage II (after the frequency jump) where dual subharmonics are present.

Constant U, varying L

Pressure spectra for selected non-dimensional impingement lengths L/θ_0 (where θ_0 is the momentum thickness at separation) and constant free-stream velocity U are shown in figure 3. (These spectra are representative of a much larger family of spectra taken at finer increments of $4\theta_0$.) The plot of dimensionless frequencies of peaks in these spectra, as a function of length, is given in figure 4. In examining figures 3 and 4, it is seen that, at shorter lengths, the energy is concentrated at the fundamental frequency β_{I}. As the length is increased, the frequency of the fundamental decreases. With a further increase in length, a component appears at $0{\cdot}5\beta_{\mathrm{I}}$. The frequency of the $0{\cdot}5\beta_{\mathrm{I}}$ component decreases proportionally with that of the β_{I} component as length is increased, until the critical length, at which the frequency jump occurs. At $L/\theta_0 = 98$ in figures 3 and 4, the fundamental has jumped to β_{II}, producing two well-defined frequency components at about $0{\cdot}4\beta_{\mathrm{II}}$ and about $0{\cdot}6\beta_{\mathrm{II}}$, as well as two components at about $0{\cdot}2\beta_{\mathrm{II}}$ and about $0{\cdot}8\beta_{\mathrm{II}}$, which become very weak and disappear at short distances from the jump. These components ($0{\cdot}2\beta$, $0{\cdot}8\beta$) cannot be considered significant; consistent phase measurements were not possible at these frequencies.

At the jump, the extension of the $0{\cdot}5\beta_{\mathrm{I}}$ component into stage II appears as the component at about $0{\cdot}4\beta_{\mathrm{II}}$, suggesting that the same mechanism may be responsible for the production of both components. Discussion of the $0{\cdot}6\beta_{\mathrm{II}}$ component will be delayed until after the results of the fixed impingement length with varying free-stream velocity are presented.

Figure 5 shows amplitude data corresponding to the frequency data of figure 4. In stage I, the onset of cavity oscillations is quite distinct. As the impingement length is increased, the amplitude of the β_{I} component grows quickly, saturates, and decays as the $0{\cdot}5\beta_{\mathrm{I}}$ component appears and extracts energy from the β_{I} component. At $L/\theta_0 \simeq 97$ the frequency of the fundamental component jumps to a higher value. There is little change in amplitude of the component at the fundamental frequency; that is $A_{\beta_{\mathrm{I}}} \simeq A_{\beta_{\mathrm{II}}}$ at the jump. The $0{\cdot}5\beta_{\mathrm{I}}$ component reaches its maximum amplitude just prior to the jump. In stage II there is considerable scatter in the data, most likely resulting from a degree of intermittency of the subharmonics. In general, it is seen that the strength of the β_{II} component slowly decays and the subharmonics slowly gain strength, until $L/\theta_0 \simeq 145$. The low-frequency components at $0{\cdot}5\beta_{\mathrm{I}}$ and at about $0{\cdot}4\beta_{\mathrm{II}}$ and $0{\cdot}6\beta_{\mathrm{II}}$ are always of the same order of magnitude; typically they are a substantial fraction of the corresponding fundamental component. This observation

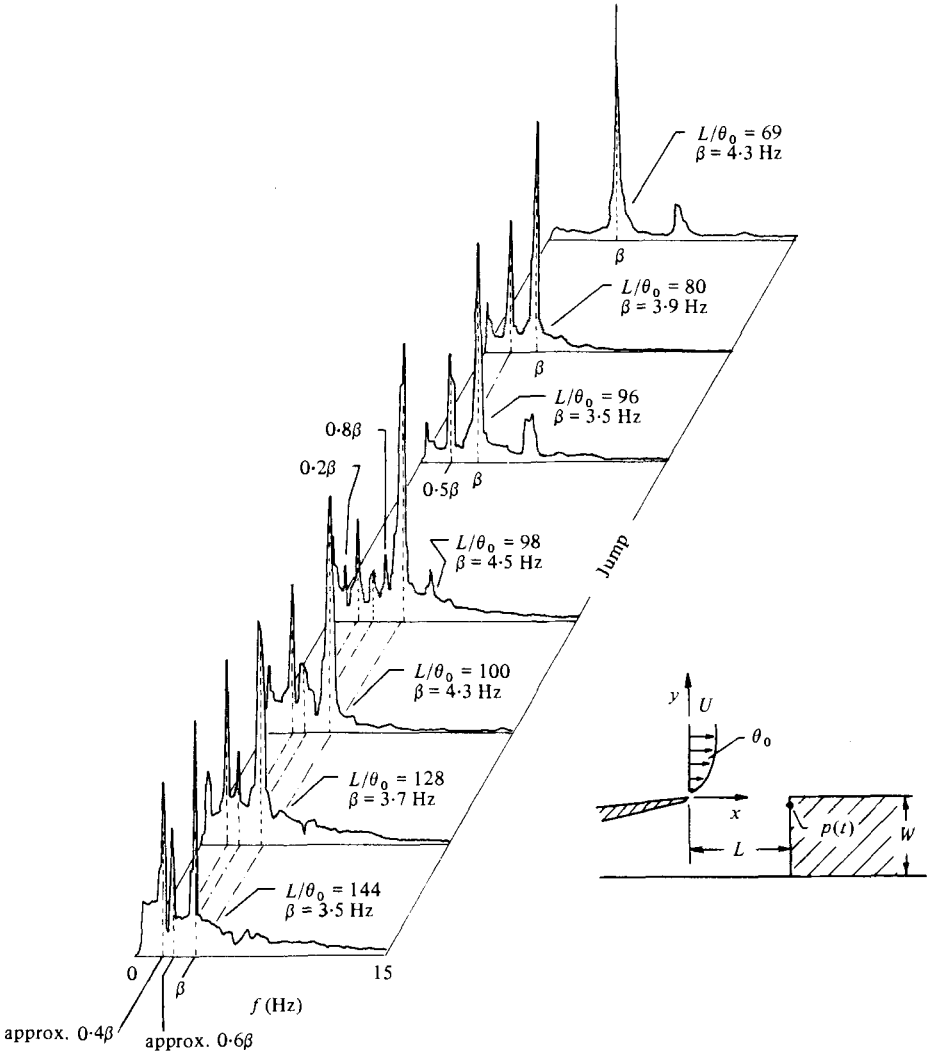

FIGURE 3. Fluctuating-pressure spectra for increasing impingement length showing jump from stage I to stage II; $R_{\theta_0} = 190$.

underscores the necessity of considering the dynamics of the subharmonic component(s) in characterizing the unsteady flow field.

Varying U, fixed L

Further insight into the oscillation process, and corroboration of the data obtained for variation of impingement length, was attained by varying the free-stream velocity U at a constant value of length L. Figure 6 shows selected spectra and figure 7 portrays behaviour of the peak frequencies as a function of velocity for the larger family of spectra from which those of figure 6 were extracted. These spectra were obtained using the ramp in figure 2 (*b*). In figure 6, the $0{\cdot}5\beta_{\mathrm{I}}$ component does not appear at the lowest velocity, but, as U is increased, the $0{\cdot}5\beta_{\mathrm{I}}$ component appears as a significant spectral component. As indicated in figure 7, at a sufficiently high flow speed, the

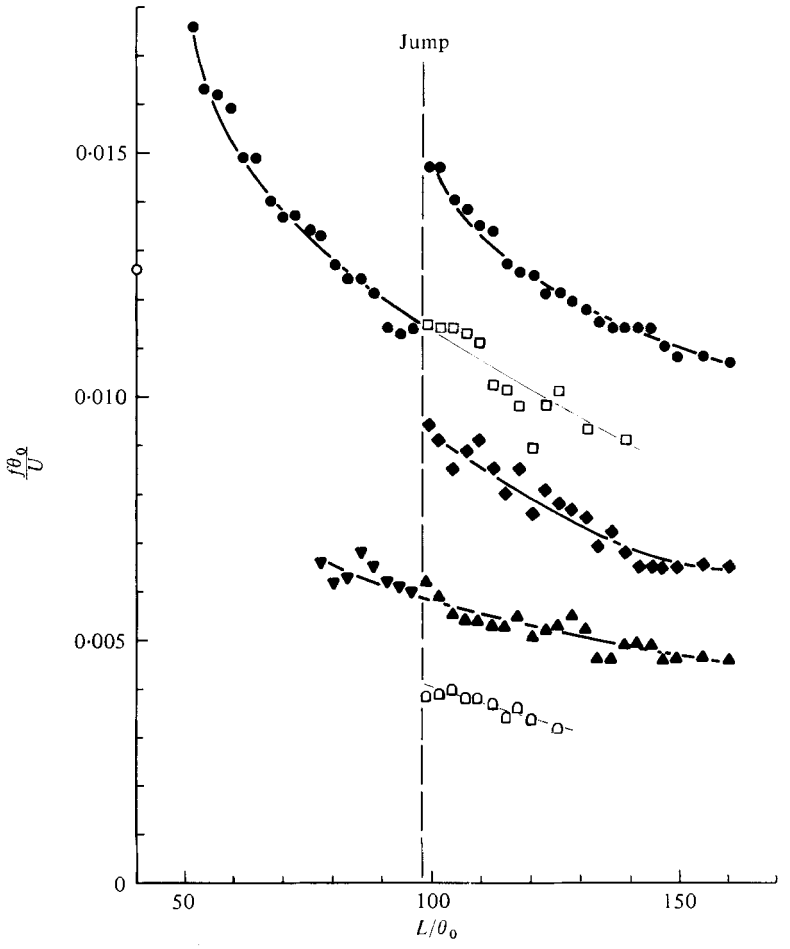

FIGURE 4. Peak (non-dimensionalized) frequencies of pressure-fluctuation spectra as functions of impingement length, showing multiple low-frequency components in stage II; $R_{\theta_0} = 190$. Solid symbols indicate predominant and persistent components. ●, β; □, $0{\cdot}8\beta$; ◆, $0{\cdot}6\beta$; ▼, $0{\cdot}5\beta$; ▲, $0{\cdot}4\beta$; ⍁, $0{\cdot}2\beta$.

frequency jump occurs and characteristic stage II oscillations are present (not shown in figure 6). However, decreasing the velocity to the point at which the jump had occurred with increasing velocity does not produce a jump back to stage I. Instead, the stage II oscillations, nominally $0{\cdot}4\beta_{II}$, $0{\cdot}6\beta_{II}$ and β_{II}, persist throughout the region that had been characterized by severe $0{\cdot}5\beta_I$ modulation with increasing velocity. At a much lower speed the flow reverts to stage I behaviour. This marked difference between data acquired with increasing and decreasing velocity indicates the occurrence of strong hysteresis, for not only the fundamental (β) but also its subharmonics ($0{\cdot}4\beta$, $0{\cdot}6\beta$). The hysteresis region is outlined in figure 7, with arrows indicating the sequence in which the data were obtained. The occurrence of hysteresis for this case of fixed L and changing U indicates the presence of two bistable modes in the region of the frequency jump and underscores the importance of considering the history of the flow system in characterizing its dynamic behaviour.

In figure 7, as in figure 4, the $0{\cdot}4\beta_{II}$ component appears as an extension of the $0{\cdot}5\beta_I$

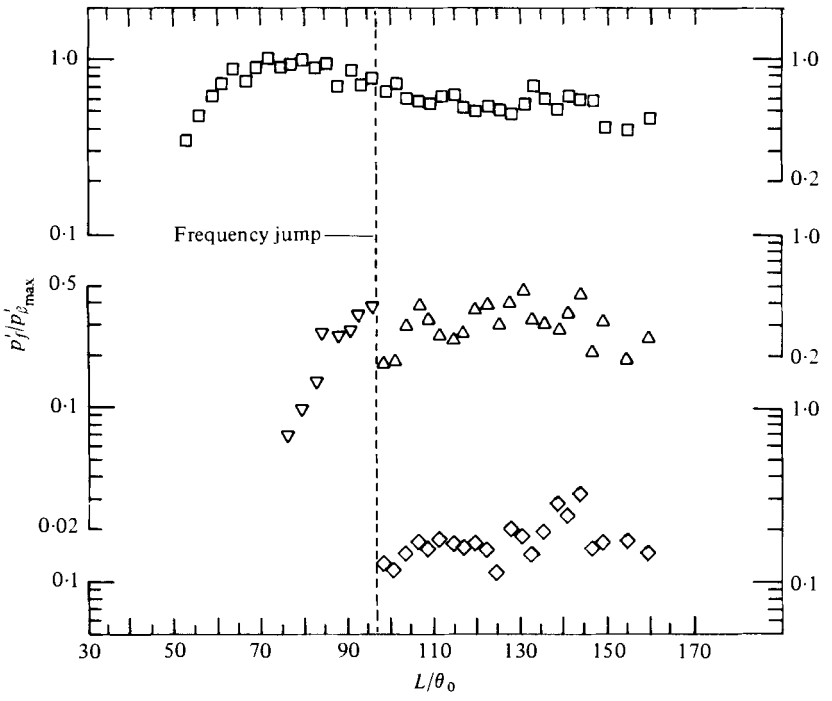

FIGURE 5. Amplitudes of fluctuation of predominant frequency components as functions of impingement length; $R_{\theta_0} = 190$. □, β; △, approx. $0{\cdot}4\beta$; ▽, $0{\cdot}5\beta$; ◇, approx. $0{\cdot}6\beta$.

component into stage II. The component at about $0{\cdot}6\beta_{II}$, occurring in stage II in figures 4 and 7, is felt to be associated with nonlinear wave interaction. In essence, it is well known, from dual-frequency (f_a and f_b) external excitation of free shear layers, that the nonlinear interaction of two discrete frequencies (f_a, f_b) can produce various combination modes corresponding to $f_a - f_b$ etc. (see, for example, Sato 1971; Miksad 1973; Ronneberger & Ackermann 1979). In a given experiment, it will be the survivors of the nonlinear mode competition that are detectable in a given series of measurements. Employing this concept, the generation of the $0{\cdot}6\beta_{II}$ component observed herein may be attributed to the interaction of the component at about $0{\cdot}4\beta_{II}$ with β_{II}; that is, the component at about $0{\cdot}6\beta_{II}$ corresponds to the difference frequency. Also significant is the fact that the $0{\cdot}4\beta_{II}$ component is always stronger than the $0{\cdot}6\beta_{II}$ component (see figure 5), supporting the concept of generation of the $0{\cdot}6\beta_{II}$ component through nonlinear interaction of the two stronger components at about $0{\cdot}4\beta_{II}$ and at β_{II}. Section 4 examines nonlinear interaction in detail.

4. Nonlinear interaction: bispectral analysis

The term 'nonlinear interaction' has been applied to phenomena that involve coupling between two frequencies to produce a third. Necessary conditions for this 'three-wave coupling' between waves of frequencies (f_1, f_2, f_3) and wavenumbers (k_1, k_2, k_3) are the frequency (i.e. $f_1 + f_2 = f_3$) and the wavenumber (i.e. $k_1 + k_2 = k_3$) selection rules (Kim & Powers 1979). However, these selection rules for f and k may also be satisfied by self-excited independent-wave phenomena. If f_3 is a normal mode,

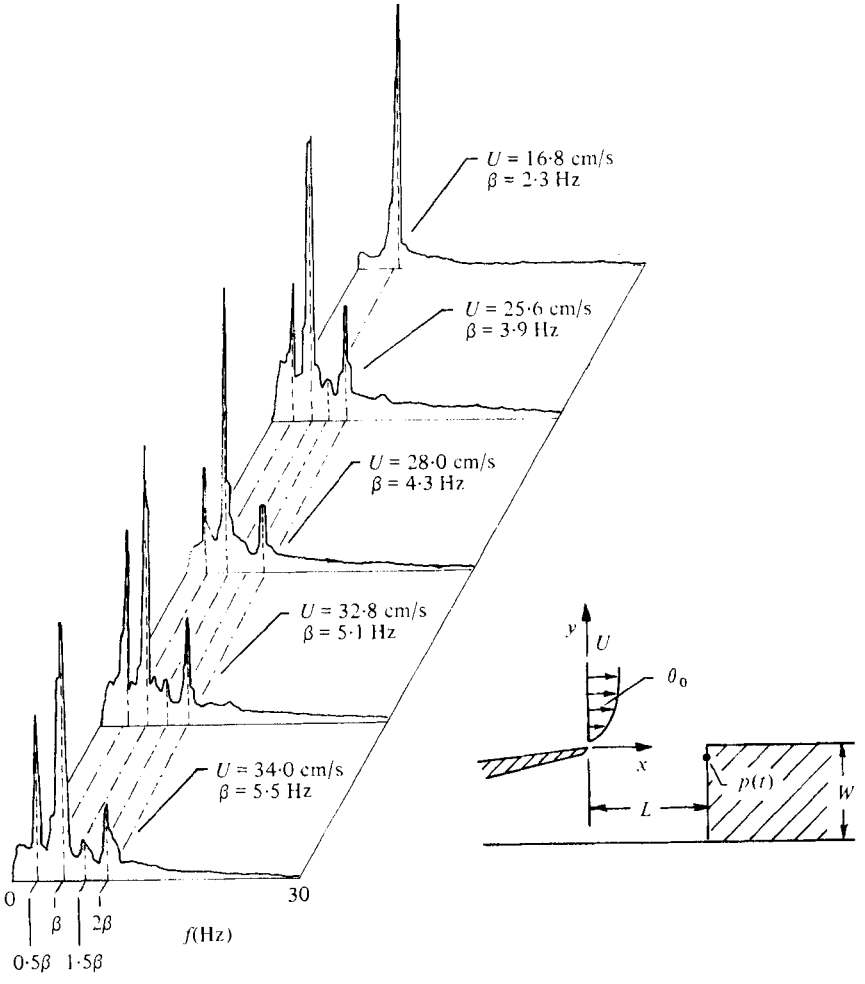

FIGURE 6. Fluctuating-pressure spectra for increasing velocity (with L = 6 cm, fixed) showing stage I oscillations.

and not a product of nonlinear interaction, it is not expected to have any phase coherence with the fluctuations at frequencies f_1 and f_2.

To a first approximation, any signal which fluctuates in time (hereafter referred to as a time series) and is assumed to be a linear superposition of statistically independent frequency components, may be described by its power (or amplitude) spectrum, which indicates the frequency† distribution of power (or amplitude) of the fluctuations. If the assumption that the process is a linear superposition of statistically independent frequency components is valid, the power spectrum then describes the process completely (Blackman & Tukey 1958). For nonlinear phenomena, second-order (power) spectra do not provide sufficient information for a thorough examination of the nonlinear aspects (Rosenblatt & Van Ness 1965). Investigation of these processes requires third- and higher-order moment functions and their transforms. The third-order

† The term 'frequency' is used throughout this discussion in the sense of the number of cycles per second of a sinusoid (Hz) and not in the statistical sense.

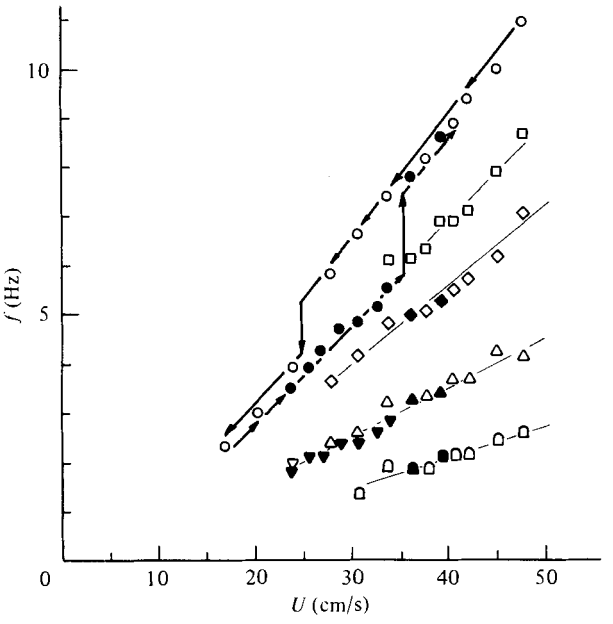

FIGURE 7. Peak frequencies of pressure-fluctuation spectra as functions of free-stream velocity, showing hysteresis region. For decreasing U: ○, β component; □, $0{\cdot}8\beta$; ◇, $0{\cdot}6\beta$; ▽, $0{\cdot}5\beta$; △, $0{\cdot}4\beta$; ⌂, $0{\cdot}2\beta$. Corresponding solid symbols are for increasing U.

spectrum, known as the bispectrum, has been used as a tool in studies of nonlinear interactions in oceanographic (Hasselmann, Munk & MacDonald 1963) and plasma physics (Kim & Powers 1978, 1979; Kim *et al.* 1980) applications, as well as in studies of sunspot activity (Brillinger & Rosenblatt 1967), and in determining the non-locality of the turbulent energy cascade (Lii, Rosenblatt & Van Atta 1976). The bispectrum and its normalized counterpart, the bicoherence spectrum, provide a means through which (quadratic) nonlinear interactions may be examined and quantified. To define the bicoherence spectrum, it is first necessary to recall the definition of power spectrum and then define the bispectrum, since both of these quantities are used in the definition of bicoherence spectrum. To do this, define a real and stationary signal $x(t)$ with a zero mean value and a Fourier representation

$$x(t) = \sum_{k=-\infty}^{\infty} X_k e^{-i\omega_k t},$$

$$X_k = \lim_{T\to\infty} \frac{1}{T} \int_{-\frac{1}{2}T}^{\frac{1}{2}T} x(t)\, e^{i\omega_k t}\, dt,$$

where $X_{-k} = X_k^*$ ($*$ indicates complex conjugate), $\omega_k = 2\pi k/T$, and T is the record length of $x(t)$.

The power spectrum of the time series may be written (to within a constant) as

$$P(k) = \lim_{T\to\infty} E[X_k X_k^*]$$

where $E[\ ]$ denotes a mean (or expected) value. The power spectrum indicates the contribution to the mean square $E[x^2(t)]$ from those spectral components at f_k of width Δf, where $\Delta f = 1/T$, and $f_k = \omega_k/2\pi = k/T$.

Similarly, the bispectrum may be defined as

$$B(k,l) = \lim_{T\to\infty} E[X_k X_l X^*_{k+l}],$$

and represents the contribution to the mean cube value of those spectral components at f_k and f_l of area $(\Delta f)^2$. As stated by Kim & Powers (1978), the bispectrum could alternatively be defined as the two-dimensional Fourier transform of a second-order correlation function $C(\tau_1, \tau_2) = E[x(t)\,x(t+\tau_1)\,x(t+\tau_2)]$.

The bicoherence spectrum is a normalized version of the bispectrum, and is defined in a manner analogous to the linear coherence spectrum, which measures, on a spectral basis, the degree of linear correlation between two signals (Kim & Powers 1979). The definition of the bicoherence spectrum to be used in this study is

$$b^2(k,l) = \frac{|B(k,l)|^2}{P(k)\,P(l)\,P(k+l)},$$

in which B and P represent the bispectrum and power spectrum defined earlier and k and l are integers representing the kth and lth discrete frequency components, i.e. $f_k = (k-1)\,\Delta f$ and $f_l = (l-1)\,\Delta f$.

The value of the bicoherence spectrum is expected to lie between zero and unity (Kim & Powers 1979). When nonlinear coupling and phase coherence are present, the bicoherence spectrum (hereinafter also referred to simply as the bicoherence) will take on a value near unity. A value of the bicoherence near zero would indicate the three components f_k, f_l, f_{k+1} to be independent, self-excited modes. Further, for intermediate values, Kim & Powers (1979) have shown that the value of the bicoherence may be interpreted as the fraction of power present at the interaction frequency that is due to quadratic coupling between the two component frequencies.

The above definition of bicoherence appears in the literature (Kim & Powers 1978) and has been used in calculations of bicoherence estimates (Haubrich 1965); estimates obtained using this definition are not necessarily bounded by unity. If it is desired to ascertain that the maximum value of $b^2(k,l)$ is unity, one should use the following definition of bicoherence:

$$b^2 = \frac{|B(k,l)|^2}{E[|X_k X_l|^2]\,E[|X_{k+l}|^2]}.$$

Implementation of this definition in a computer algorithm requires the storage of an additional complex array $E[|X_k X_l|^2]$; in the present study, it would have resulted in a reduction of the frequency resolution because of computer limitations. Since the accurate determination of frequency components, sometimes separated by only 0·7 Hz (in stage II), was paramount, and since it is the relative degree of nonlinear coupling (i.e. relative magnitudes of bispectral peaks) that is of interest here, the first definition of $b^2(k,l)$ was employed. The computer algorithm employing the first definition of $b^2(k,l)$ successfully determined the extent of nonlinear coupling in all of the test cases of Kim & Powers (1979). In addition, in estimating the bicoherence of the experimental data, the maximum value of $b^2(k,l)$ was never observed to exceed unity.

It is noted that, because of the symmetry of the Fourier components ($X_{-k} = X^*_k$) and the limits of the Nyquist frequency because of digitization, it is only necessary to calculate the bicoherence in a triangular domain given by $0 \leqslant l \leqslant \frac{1}{4}N$, $l \leqslant k \leqslant \frac{1}{2}N - l$,

where N is the number of points in the time series. Further details of the calculation procedure may be found in Kim & Powers (1979) and Knisely (1980).

The same symmetry relation for Fourier components results in the following symmetry relations for the bicoherence:

$$b^2(k,l) = b^2(l,k) = b^2(-k,-l),$$
$$b^2(k,l) = b^2(-k-l,l) = b^2(k,-k-l),$$
$$b^2(k,l) = b^2(-l,k+l) = b^2(-k,k+l).$$

In applying the bicoherence calculations to the impinging cavity shear layer, two representative impingement lengths were chosen, corresponding to conditions before (single subharmonic) and after (dual subharmonic) the frequency jump. The criteria for choosing each of these lengths was existence of a well-defined $0{\cdot}5\beta_{\mathrm{I}}$ component for the shorter length ($L/\theta_0 = 80$, stage I) and pronounced approx. $0{\cdot}4\beta_{\mathrm{II}}$ and approx. $0{\cdot}6\beta_{\mathrm{II}}$ components for the longer ($L/\theta_0 = 100$, stage II). These lengths are the same as those employed in subsequent flow visualization, measurement of growth rates, and streamwise phase variations.

The aforementioned three-wave coupling criteria ($f_3 = f_1 + f_2, k_3 = k_1 + k_2$) is satisfied in stage I by the frequency components $0{\cdot}5\beta_{\mathrm{I}}$ and β_{I}, which have approximately equivalent phase speeds (as shown in § 7), indicating that their one-dimensional wavenumbers satisfy the coupling criterion. In stage II, the coupling criteria are satisfied by approx. $0{\cdot}4\beta_{\mathrm{II}}$, approx. $0{\cdot}6\beta_{\mathrm{II}}$ and β_{II}, whose phase speeds are again approximately equivalent (see § 7).

To account for the observed intermittency of strong subharmonic components, a form of 'conditional sampling' is employed. It involves examination of the spectrum of each individual record to find those records that have strong subharmonic modulation exceeding a defined threshold. Once these records are identified, their spectra and bicoherence spectra are averaged together to give a 'conditionally averaged' spectrum and bicoherence spectrum for each of the two representative lengths investigated here.

The 'sampling criterion' involved selection of records whose spectra showed low-frequency amplitude peaks at least 35 % of the amplitude of the corresponding fundamental. This criterion was satisfied by four records (for each impingement length) of velocity fluctuations at the edge of the shear layer within the domain $10 \leqslant x/\theta_0 \leqslant 30$, thereby providing a spatially averaged bicoherence. The same sampling criterion was used for both impingement lengths, and calculations were executed using the CDC 6400 computer.

In the following, the two representative cases are considered: first, the shorter impingement length, giving rise to a *single subharmonic* at $0{\cdot}5\beta_{\mathrm{I}}$; then, the longer length, associated with the *dual subharmonic* at about $0{\cdot}4\beta_{\mathrm{II}}$ and about $0{\cdot}6\beta_{\mathrm{II}}$.

Single subharmonic

First, the case of subharmonic modulation at a single frequency will be examined. Modulation at $0{\cdot}5\beta_{\mathrm{I}}$ is exhibited in the signals shown in figure 8. These signals are taken from the records whose spectra were averaged together to produce the 'conditionally averaged' spectrum shown in figure 9 (*a*). In this spectrum, the half-harmonic ($0{\cdot}5\beta_{\mathrm{I}}$) component has a magnitude in excess of 40 % of the amplitude of the fundamental. Figures 9 (*b*, *c*) present the 'conditionally averaged' bicoherence spectrum,

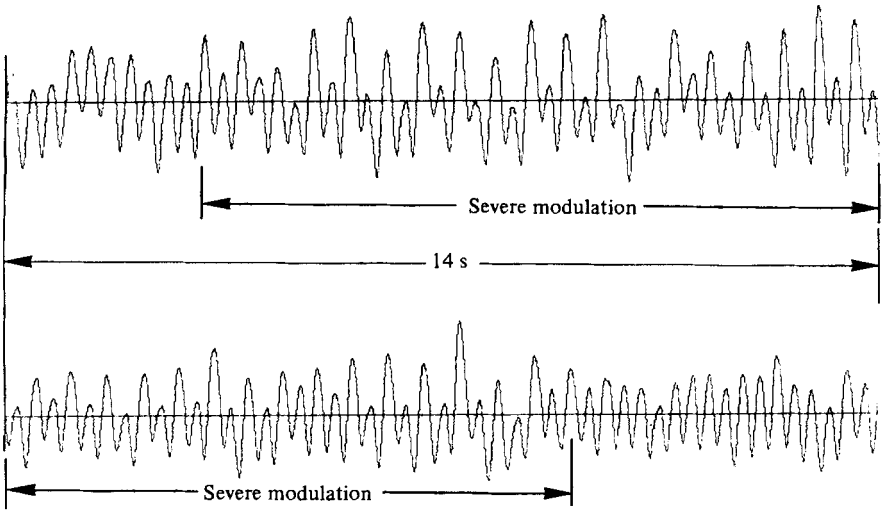

FIGURE 8. Instantaneous traces from 'conditionally sampled' data, showing strong modulation at one-half the fundamental frequency ($0{\cdot}5\beta$); $L/\theta_0 = 80$; $R_{\theta_0} = 190$.

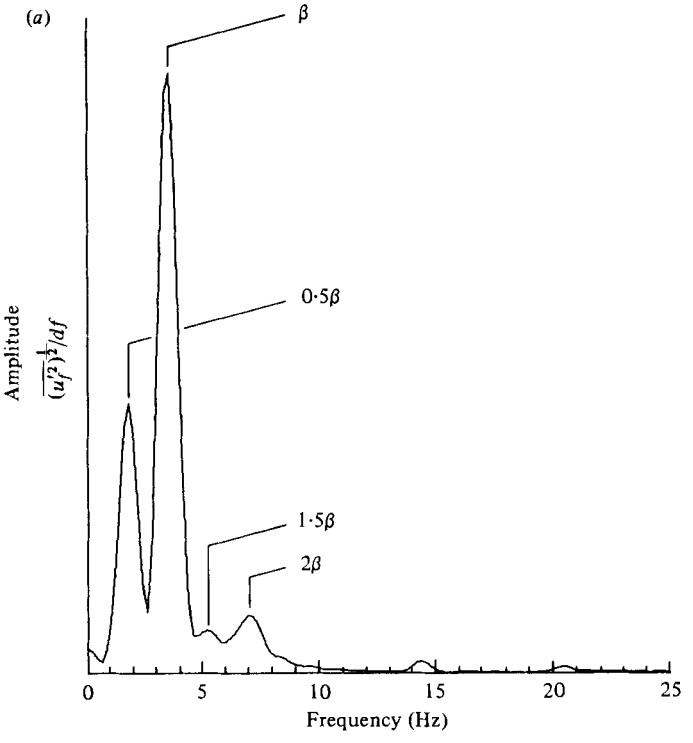

FIGURE 9. For legend see facing page.

in the form of both perspective and contour plots. From the contour plot (figure 9*c*), it is easily seen that interaction peaks exist at $(0{\cdot}5\beta_I, 0{\cdot}5\beta_I)$, $(\beta_I, 0{\cdot}5\beta_I)$, (β_I, β_I), $(1{\cdot}5\beta_I, 0{\cdot}5\beta_I)$ and $(2\beta_I, \beta_I)$. Owing to symmetry relations (Knisely 1980), there are two possible interpretations of the peak at $(0{\cdot}5\beta_I, 0{\cdot}5\beta_I)$:

$$0{\cdot}5\beta_I + 0{\cdot}5\beta_I \rightarrow 1{\cdot}0\beta_I, \quad 1{\cdot}0\beta_I - 0{\cdot}5\beta_I \rightarrow 0{\cdot}5\beta_I.$$

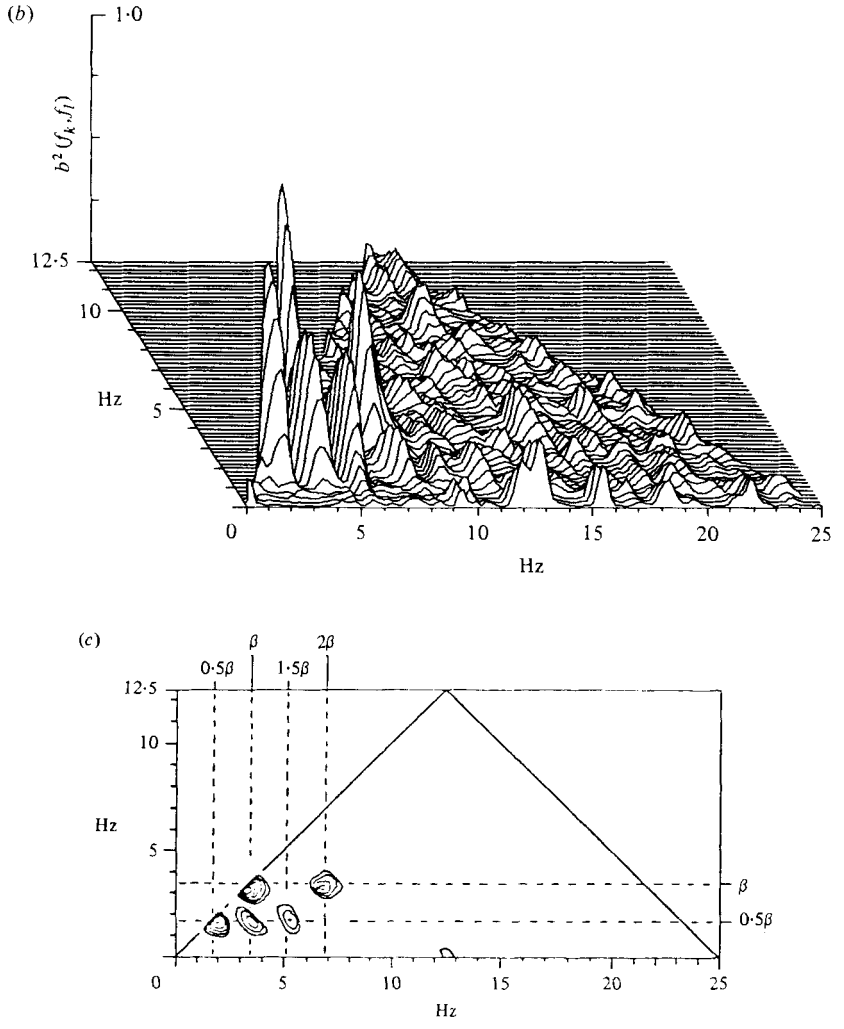

FIGURE 9. Time-averaged (*a*) amplitude spectrum, (*b*) perspective view of bicoherence spectrum and (*c*) top (contour) view of bicoherence spectrum for 'conditionally sampled' data, showing characteristic stage I oscillations with modulation at $0{\cdot}5\beta$. In (*c*), initial contour value is 0·20, with an increment of 0·15 between contours; $L/\theta_0 = 80$, $R_{\theta_0} = 190$.

In this notation, the symbol $\rightarrow$ represents the phrase 'produces through nonlinear interaction'. In the first interpretation, the half-harmonic couples with itself to produce the fundamental. Since the fundamental component is known to arise from inherent shear-layer instability, and, as was shown in figure 3, the fundamental can exist alone without subharmonics at shorter cavity lengths, this interpretation appears somewhat inconsistent. In the second interpretation, derived from the symmetry relation $b^2(k,l) = b^2(-l, k+l)$, the peak at $(0{\cdot}5\beta_{\mathrm{I}}, 0{\cdot}5\beta_{\mathrm{I}})$ is due to the half-harmonic $(0{\cdot}5\beta_{\mathrm{I}})$ coupling nonlinearly with the fundamental (β_{I}) to reinforce the half-harmonic oscillations. The coupling term would be of the form

$$\cos(2\pi\beta_{\mathrm{I}} t + \phi_{\beta_{\mathrm{I}}}) \cos(2\pi(0{\cdot}5\beta_{\mathrm{I}})\, t + \phi_{0{\cdot}5\beta_{\mathrm{I}}}),$$

which can be rewritten in the form of sum and difference frequencies $\beta - 0{\cdot}5\beta$ and $\beta_{\mathrm{I}} + 0{\cdot}5\beta_{\mathrm{I}}$. The difference frequency then shows up in the bicoherence as the

$(0{\cdot}5\beta_{\rm I}, 0{\cdot}5\beta_{\rm I})$ peak, because of the symmetry relation. It is important to note that the sum frequency $(\beta_{\rm I}, 0{\cdot}5\beta_{\rm I})$ shows up as well in the bicoherence (although with reduced amplitude), lending support to this second interpretation.

In figures 9(*b*, *c*), the peak at $(0{\cdot}5\beta_{\rm I}, 0{\cdot}5\beta_{\rm I})$ takes a value in excess of 0·85, indicating that a large portion of the energy at $0{\cdot}5\beta_{\rm I}$ results from the difference interaction of the $0{\cdot}5\beta_{\rm I}$ component with the $\beta_{\rm I}$ component; i.e. the subharmonic modulation at $0{\cdot}5\beta_{\rm I}$ is 'self-excited' in the sense that a small disturbance at $0{\cdot}5\beta_{\rm I}$ can reinforce itself substantially through its interaction with $\beta_{\rm I}$. Kelly (1967), in analysing interactions among frequency components in an inviscid shear layer with a hyperbolic tangent profile, has shown that a disturbance at one half the frequency (subharmonic) of a periodic base flow, can interact with the base flow to reinforce the disturbance at the half-harmonic. The results of the present conditionally sampled bicoherence analysis do indeed support the concept of subharmonic reinforcement due to interaction with its fundamental. Further support is obtained by recalling the amplitude data of figure 5. The amplitude of the fundamental was seen to decrease with the appearance of the subharmonic, indicating energy flow from the fundamental to the subharmonic.

The generation of higher harmonics in shear layers is documented in the work of Browand (1966) and Miksad (1972), among others. Furthermore, it can be shown (Knisely 1980) that the production of higher harmonics is well predicted by Stuart's (1967) nonlinear inviscid solution. In the present study the peaks at $(\beta_{\rm I}, \beta_{\rm I})$ and $(2\beta_{\rm I}, \beta_{\rm I})$ in figures 9(*b*, *c*) are interpreted as the interaction of the $\beta_{\rm I}$ frequency component with itself to produce the $2\beta_{\rm I}$ frequency component, and the further interaction of the $\beta_{\rm I}$ component with the $2\beta_{\rm I}$ component to produce a component at $3\beta_{\rm I}$.

The major peaks in the conditionally averaged bicoherence spectrum (figures 9*b*, *c*) have been accounted for. Peaks at $(0{\cdot}5\beta_{\rm I}, 0{\cdot}5\beta_{\rm I})$ and $(\beta_{\rm I}, 0{\cdot}5\beta_{\rm I})$ have been shown to indicate generation of difference and sum frequencies, with the difference frequency being the low-frequency modulation component $0{\cdot}5\beta_{\rm I}$. The peaks at $(\beta_{\rm I}, \beta_{\rm I})$ and $(2\beta_{\rm I}, \beta_{\rm I})$ indicate generation of higher harmonic components.

Dual subharmonic

Similar conditional sampling and bicoherence analysis was carried out for the representative case involving two subharmonic components ($L/\theta_0 = 100$). Figure 10 presents sample segments from the velocity-fluctuation records, whose spectra were ensemble-averaged to produce the 'conditionally sampled' spectrum of figure 11(*a*). Note that the approx. $0{\cdot}4\beta_{\rm II}$ and approx. $0{\cdot}6\beta_{\rm II}$ modulation in the signals produces a five-cycle repetitive pattern. The five-cycle repetition is denoted by the pattern *ab* or *a'b'*; the changing nature of the five-cycle pattern is an indication of the time-dependent nature of phasing between frequency components. The conditionally averaged spectrum displays a very strong $0{\cdot}4\beta_{\rm II}$ component, having an amplitude approx. 80 % of the fundamental. The amplitude of the $0{\cdot}6\beta_{\rm II}$ component is about half that of the $0{\cdot}4\beta_{\rm II}$ component, or about 40 % that of the fundamental. The corresponding 'conditionally sampled' bicoherence spectrum (figures 11*b*, *c*) shows significant interaction, as was found for the shorter-impingement-length case.

Following the previous line of reasoning for the single subharmonic modulation and using the same symmetry relation, $b^2(k, l) = b^2(-l, k+l)$, the peaks at (approx.

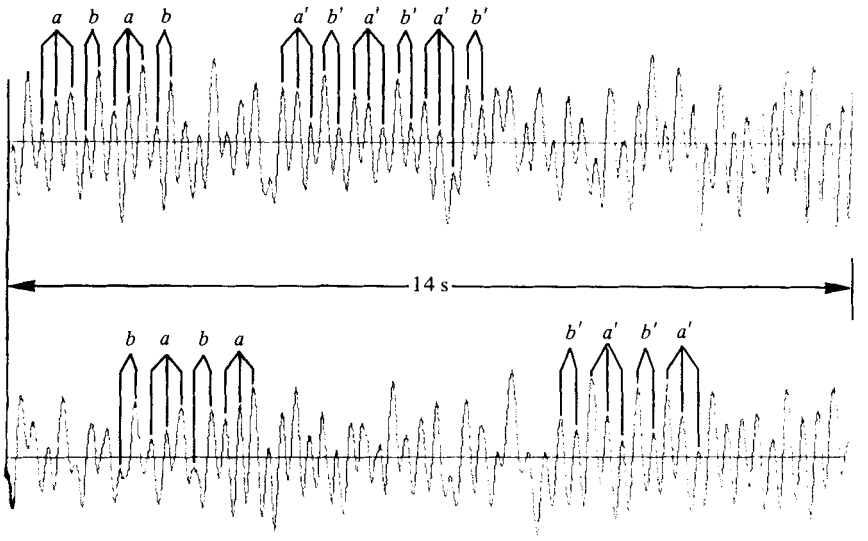

FIGURE 10. Instantaneous traces from 'conditionally sampled' data, showing 5-cycle-repetition characteristics of stage II oscillations designated by *ab* and *a'b'*; $L/\theta_0 = 100$, $R_{\theta_0} = 190$.

$0{\cdot}6\beta_{II}$, approx. $0{\cdot}4\beta_{II}$) and (β_{II}, approx. $0{\cdot}4\beta_{II}$), may be interpreted as representing an interaction of the form $\cos[2\pi(0{\cdot}4\beta_{II})t + \phi_{0{\cdot}4\beta_{II}}]\cos[2\pi\beta_{II}t + \phi_{\beta_{II}}]$. As in the single-subharmonic case, this interaction can be rewritten in terms of sum and difference frequencies $\beta_{II} - 0{\cdot}4\beta_{II}$ and $\beta_{II} + 0{\cdot}4\beta_{II}$. The difference-frequency interaction gives the peak at ($0{\cdot}6\beta_{II}$, $0{\cdot}4\beta_{II}$) and the sum interaction frequency is reflected in the peak at (β_{II}, $0{\cdot}4\beta_{II}$). As previously discussed, the moderately strong peak at (β_{II}, β_{II}) indicates generation of the $2\beta_{II}$ harmonic.

The remaining two peaks, at (approx. $1{\cdot}4\beta_{II}$, β_{II}) and (approx. $1{\cdot}4\beta_{II}$, approx. $0{\cdot}6\beta_{II}$) have several possible interpretations, none of which can be ruled out *a priori*; possible interpretations are discussed by Knisely (1980).

In summary, 'conditionally sampled' bicoherence spectra indicate that stage I and II both involve the interaction of the fundamental frequency with a low frequency at $0{\cdot}5\beta_I$ in stage I and at approx. $0{\cdot}4\beta_{II}$ in stage II. For single subharmonic modulation (at $L/\theta_0 = 80$), the interaction serves to reinforce the subharmonic modulation, demonstrating the self-sustaining nature of the subharmonic modulation. For dual-subharmonic modulation (at $L/\theta_0 = 100$), the interaction of the $0{\cdot}4\beta_{II}$ component with the β_{II} component gives rise to both sum and difference frequencies, the dominant component being the difference frequency at approx. $0{\cdot}6\beta_{II}$. For both characteristic lengths, the interaction may be written as $\cos[2\pi(\alpha\beta)t]\cos[2\pi\beta t]$, where $\alpha\beta$ is the low-frequency component. Written in this manner, it is clear that the low-frequency component (either $0{\cdot}5\beta_I$ or $0{\cdot}4\beta_{II}$) serves to amplitude-modulate the oscillation at the fundamental shear-layer-instability frequency.

The fundamental frequency is generated by the shear-layer instability. The source of the low-frequency component is apparently the result of a self-selection process, whereby a cyclic displacement of the shear layer at impingement gives rise to a low-frequency component whose overall phase difference is compatible with the cavity length. As will be shown in § 7, the lowest-frequency subharmonic component has a

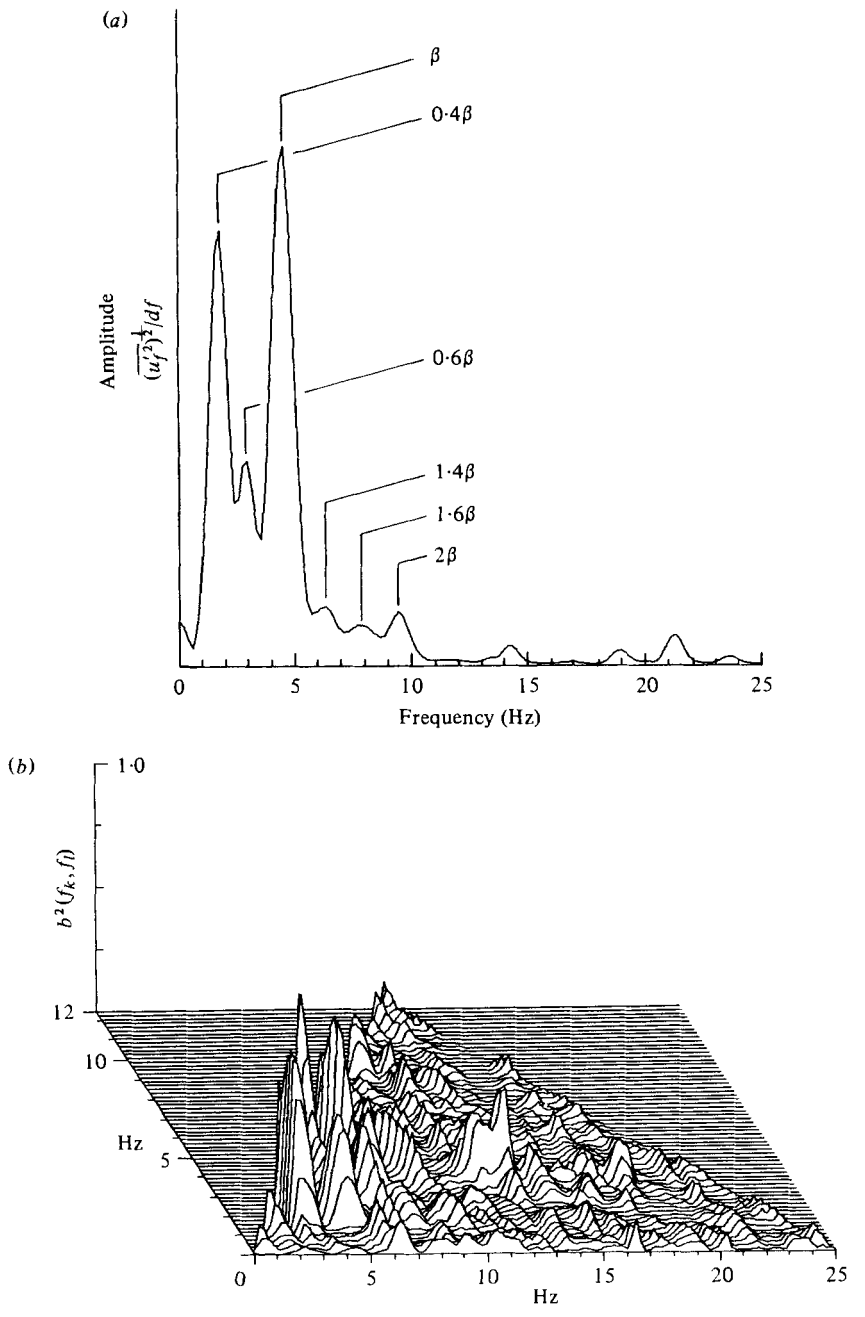

FIGURE 11. For legend see facing page.

wavelength that is equal to the impingement length for both lengths examined here, and propagates at approximately the same phase speed as the fundamental component. This low-frequency component, as will be shown in § 5, may be interpreted as a low-frequency flapping of the shear layer spanning the cavity mouth.

In addition, bicoherence analysis clearly indicates the coupling (phase coherence) associated with production of *higher* harmonics, heretofore uncharacterized on

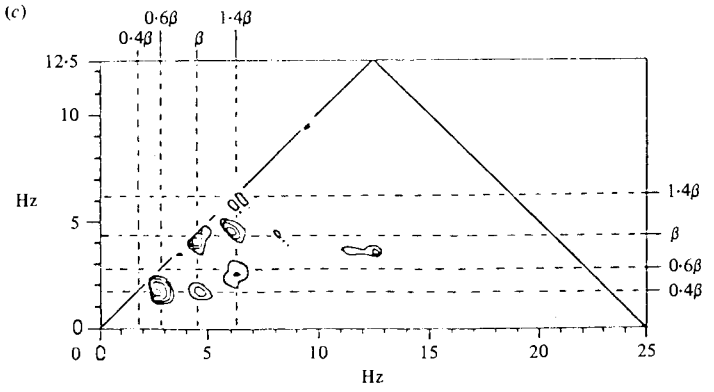

FIGURE 11. Time-averaged (*a*) amplitude spectrum, (*b*) perspective view of bicoherence spectrum, and (*c*) top (contour) view of bicoherence spectrum for 'conditionally sampled' data, showing characteristic stage II oscillations with predominant modulation at approx. $0{\cdot}4\beta$. In (*c*), initial contour value is 0·20, with an increment of 0·15 between contours; $L/\theta_0 = 100$, $R_{\theta_0} = 190$.

a bispectral basis. This higher-harmonic production has been observed in earlier studies of externally excited, non-impinging shear layers in one-dimensional spectra.

5. Source of dominant upstream influence: vortex–corner interactions

In order for the oscillation at the fundamental and low frequencies to be self-sustaining, the unsteady flow-corner interaction, and its upstream influence, must be compatible with these observed frequencies. In examining the nature of these corner interactions, extensive flow visualization was employed.

In this investigation, the existence of large vortical structures in the cavity shear layer was demonstrated using the hydrogen-bubble technique with various time-line markers; however, the electrical field required for the hydrogen-bubble electrolysis precluded use of hot-film anemometry, necessitating dye visualization. The preliminary hydrogen-bubble experiments, in conjunction with the discussion of Michalke (1965), justified the interpretation of dye-streakline roll-up as an agglomeration of vorticity. To relate the observed flow structures to pressure and velocity traces, dye visualization was combined with simultaneous anemometry and pressure measurements; this time-dependent information was recorded using the high-speed video system, discussed previously, having a framing rate of 120 frames/s. The velocity and impingement lengths were the same as those employed in the foregoing study of nonlinear interaction. The shorter length ($L/\theta_0 = 80$) is representative of stage I oscillations with modulation at $0{\cdot}5\beta_{\mathrm{I}}$. The longer length ($L/\theta_0 = 100$) corresponds to stage II oscillations with modulation at approx. $0{\cdot}4\beta_{\mathrm{II}}$.

The mechanism for generating the $0{\cdot}5\beta_{\mathrm{I}}$ component is set forth in the photographs in figure 12. Starting at the top left, working down, then up to the top right, the progress of succcessive vortices is detailed at sequential instants in time. The traces shown in figure 12 are the fluctuating pressure trace (taken at $x = L$, $y = -0{\cdot}24$ cm) and the fluctuating hot-film (located at $x = 0$ and $y = 0{\cdot}13$ cm, where $u/U = 0{\cdot}61$) trace corresponding to three cycles before and after the duration of the photographic

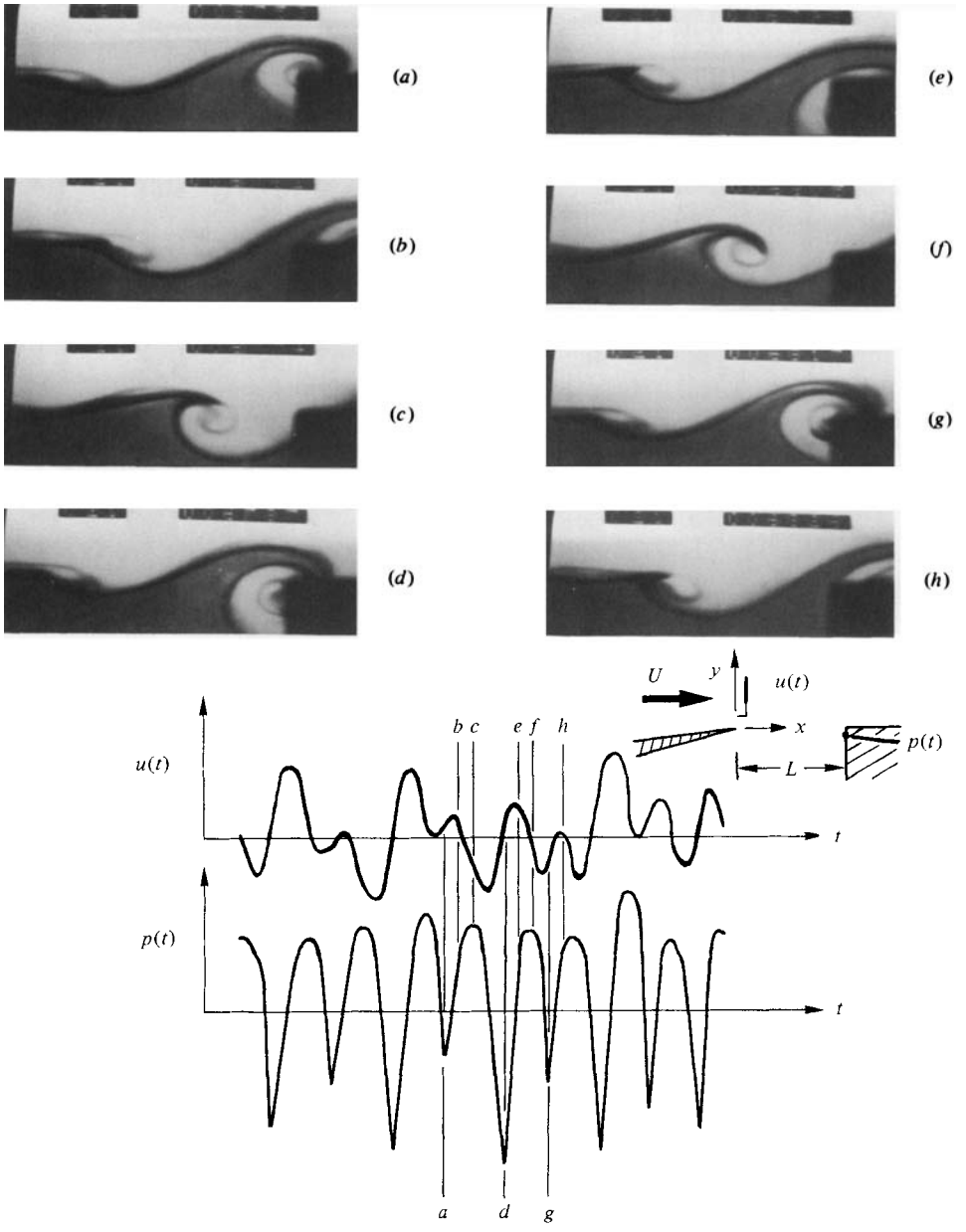

FIGURE 12. Visualization of generating mechanism at impingement for $0{\cdot}5\beta$ low-frequency modulation; $L/\theta_0 = 80$, $R_{\theta_0} = 190$.

sequence. The letters on the traces indicate the instantaneous output from the transducers corresponding to each of the photographs. In figure 12(*a*), the sharp negative-pressure spike is seen to occur when the vortex has impacted with the corner. The pressure rises to a positive maximum between successive vortices (figure 12*c*) and then drops again to an extreme negative value as the next vortex strikes (figure 12*d*). However, this second negative spike has a larger absolute magnitude than the first. A careful study of the visualization photos reveals the second vortex to be located at a lower vertical position on the edge than the first. That is, a larger fraction of the

distributed vorticity associated with the second vortex is severed by the edge. This more complete severing of the vortex results in a stronger pressure-perturbation field, which is communicated to the receptive region of the shear layer near separation, as evidenced by the hot-film trace showing the resultant velocity perturbation near separation. The third vortex in the series strikes the edge at a transverse (i.e. y) location very similar to the first and results in a smaller negative-pressure peak and smaller-amplitude upstream modulation of the shear layer. Thus it is the organized alternation in the vertical location of the vortices as they impinge on the edge that is primarily responsible for the $0{\cdot}5\beta_{\mathrm{I}}$ component observed in the spectra of stage I in figure 9(a). Moreover, the strong upstream influence of the vortex–corner interaction is seen in the velocity signal taken near separation (see figure 12).

This high–low pattern of vortex impingement was observed for as many as thirty consecutive vortices. However, this pattern was observed to alternate with a pattern involving relatively consistent impingement of vortices at the same vertical location, thereby generating pressure and velocity signals of frequency β_{I} with no noticeable low-frequency distortion. The relative duration of each of these two patterns was not constant. It is this intermittent alternation between patterns that makes cautious interpretation of time-averaged amplitudes essential.

The generation of low-frequency components in stage II also involves single-vortex–edge interaction but, as deduced from extensive visualization, the generation of low-frequency components is not due simply to a repeating high–low impingement pattern of alternate vortices. Instead, it involves cycling between varying degrees of severing of the incident vortex (see the complete-clipping, partial-clipping, and complete-escape mechanisms shown in Rockwell & Knisely 1979a). A complication in attempting to define this mechanism is that the cores of vortices impinging upon the corner at this longer length have become somewhat less organized. Although the resultant pressure signal indicates a defined pattern of interaction, the pattern is most evident from examination of the velocity fluctuations measured using a hot film at the edge of the shear layer, a technique commonly used to determine large-scale coherence in free shear layers (Lau, Fisher & Fuchs 1972; Winant & Browand 1974; Browand & Weidman 1976).

The corresponding pattern of vortex–corner interaction involves ordered interaction of five successive vortices, corresponding to five cycles of the velocity (or pressure) signal at the fundamental frequency; this vortex pattern and consequently the form of the velocity trace tended to be repetitive. The pattern of vortex–corner interaction is given in figure 13, where the horizontal line in the upper-right-hand corner of each photograph designates the hot-film probe that gave the trace at the bottom of the figure. As in figure 12, starting at the top left, working down and then up to the top right, the photos are a sequence taken from a video recording. The letters on the trace indicate the instantaneous output of the hot-film probe corresponding to each photo. The distance between the dyed region and the fixed hot-film probe indicates, in an approximate sense, the transverse (i.e. y) location of the impinging vortex. In figure 13(a), the boundary of the dyed region nearly touches the probe, and the hot-film trace shows a correspondingly large positive perturbation in velocity. In figure 13(c) there is a greater distance between the edge of the dyed region and the probe, corresponding to a relatively weak velocity fluctuation. At position (e) the trace again shows a large peak, and the dyed region in figure 13(e) again nearly touches the probe.

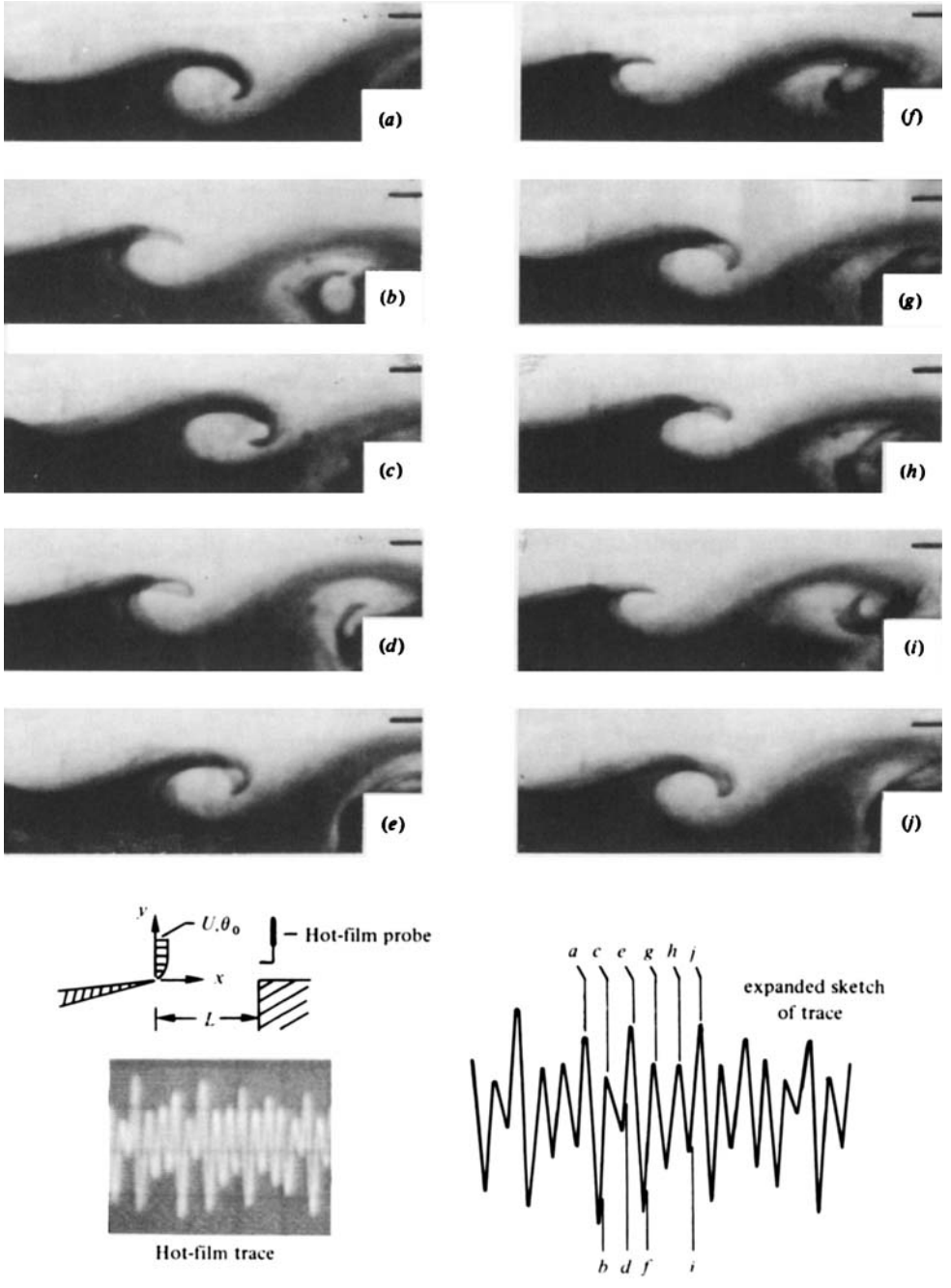

FIGURE 13. Visualization of generating mechanism at impingement for $0{\cdot}4\beta$, $0{\cdot}6\beta$ low-frequency modulation; $L/\theta_0 = 100$, $R_{\theta_0} = 190$.

In figures 13(g,h) there is more complete severing of the vortical structure, with greater distance between the probe and the dye. The corresponding velocity fluctuation is reduced. Finally, in figure 13(j) the vortex strikes the edge in a manner very similar to that portrayed in figure 13(a). From the trace, it is seen that the cycle has begun again with the occurrence of the peak labelled j.

Several features of this pattern are noteworthy. First, the velocity trace in figure 13 shows a great similarity to the traces presented in figure 10. The peaks *c*, *e*, *g*, *h*, *j* in figure 13 correspond to the pattern *ba* in figure 10. From the traces in figure 10, strong nonlinear coupling between $0{\cdot}4\beta_{II}$ and β_{II} was deduced, indicating that the process involved is *not* a simple superposition of low-frequency shear-layer flapping and shear-layer instability. Instead the process involves the amplitude modulation of the shear-layer instability by the low-frequency flapping of the shear layer.

In a simple model of this amplitude modulation, Knisely (1980) has shown that varying the relative phasing between frequency components results in five-cycle patterns with different forms. The variation of the form of the five-cycle patterns in figures 10 and 13 then suggests that the phasing between frequency components may vary significantly with time over very long records. A time-dependent phase relation is most likely associated with the observed intermittency of the stage II subharmonic self-modulation, as well as that already noted for stage I self-modulation.

Furthermore, in a related numerical study, Conlisk & Rockwell (1982) have shown that by prescribing transversely staggered patterns of vortices similar to those of figure 13, time-averaged spectra having well-defined peaks at $0{\cdot}4\beta$, $0{\cdot}6\beta$ and β can be calculated.

From the flow-visualization studies presented here, it is seen that the mechanism generating the low-frequency component is an ordered pattern of vortex–corner interactions, which may be interpreted as a low-frequency 'flapping' of the shear layer. To sustain the low-frequency modulation process, these disturbances are essentially transmitted instantaneously to the sensitive region of the shear layer at the upstream separation edge; these perturbations, in turn, are amplified as they travel downstream. Section 6 will examine the growth of this downstream-travelling wave.

6. Growth of downstream-travelling instability wave

To characterize the influence of vortex–edge interactions at impingement on the upstream flow dynamics near separation (i.e. small values of x in figure 2), it is necessary to determine the growth rates of the fundamental and low-frequency components for this region, and whether the low-frequency components grow at a rate corresponding to their own respective frequencies, or follow the growth rate of the fundamental. Growth rates of all components were determined by spectral analysis of velocity fluctuations. Each spectrum used for deducing the amplitudes of the oscillation components represented an ensemble-average of ten spectra, with each of these spectra, in turn, based on 25 cycles of oscillation. Two sets of data were taken: one with the probe positioned at the edge of the shear layer ($u/U = 0{\cdot}95$), the other with the probe at the transverse (y) location corresponding to the maximum velocity fluctuation amplitude in the shear layer. For each set, distributions of fluctuation amplitude $[\overline{(u_f')^2}]^{\frac{1}{2}}/df$ as a function of streamwise co-ordinate x could be constructed. The same two impingement lengths previously used for visualization and nonlinear interaction studies ($L/\theta_0 = 80$ and 100), corresponding to well-defined oscillations with $0{\cdot}5\beta_I$ and $0{\cdot}4\beta_{II}$ modulation, respectively, were again employed for this test.

For the case of modulation at $0{\cdot}5\beta_I$ ($L/\theta_0 = 80$), the growth of the fundamental component, measured both at the edge of the shear layer (figure 14) and at the y-location of maximum fluctuation (figure 15) agrees well with the predicted growth

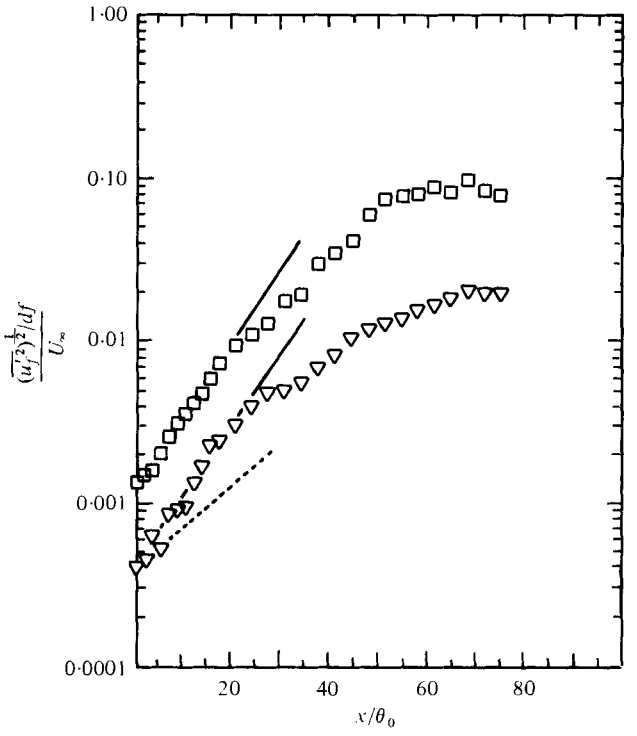

FIGURE 14. Growth rates of $0{\cdot}5\beta_{\mathrm{I}}$ and β_{II} components with increasing downstream distance; from spectral analysis of hot-film output with probe located at y-location corresponding to $u/U = 0{\cdot}95$. $R_{\theta_0} = 190$, $L/\theta_0 = 80$. $0{\cdot}5\beta$-component: ∇, data; – – – –, theory. β-component: $\square$, data; ——, theory.

rate from Michalke's (1965) linear spatial-stability theory. (The reference momentum thickness used in the theoretical calculations was the value at $x/\theta_0 = 10$, near the centre of the linear-growth region and denoted by θ_{m}.) The initial growth rate of the component at $0{\cdot}5\beta_{\mathrm{I}}$ is seen to follow closely that of the fundamental β_{I} rather than the theoretical growth rate at frequency $0{\cdot}5\beta_{\mathrm{I}}$. Moreover, the degree of half-harmonic modulation of the fundamental signal varies little in the linear region, as is reflected by the approximately parallel growth rates of β_{I} and $0{\cdot}5\beta_{\mathrm{I}}$ in figures 14 and 15. Remarkable are the relatively large initial amplitudes of the fundamental (β_{I}) and modulation ($0{\cdot}5\beta_{\mathrm{I}}$) components very near separation. At $x = 0+$ in figure 14, the respective values are $0{\cdot}0028U_\infty$ and $0{\cdot}0006U_\infty$. The 'feedback' from the region of the impingement corner is indeed strong enough to provide a substantial signal level in the 'sensitive' region of the shear layer.

For the case of modulation of the fundamental β_{II} by the $0{\cdot}4\beta_{\mathrm{II}}$ component (figures 16, 17), the linear-growth regions exhibit similar characteristics as for the modulation of β_{I} by the $0{\cdot}5\beta_{\mathrm{I}}$ component (figures 14, 15): the low-frequency components follow the growth rate of the fundamental. However, the amplitudes of all components at $x = 0^+$ are considerably weaker for the longer-length cavity (compare figures 14, 15 with 16, 17), indicating a weaker upstream influence from the impingement edge. Most significant is that all components in figures 16 and 17 are of the same order of magnitude at $x = 0^+$, with the $0{\cdot}4\beta_{\mathrm{II}}$ and β_{II} components being nearly equal. More-

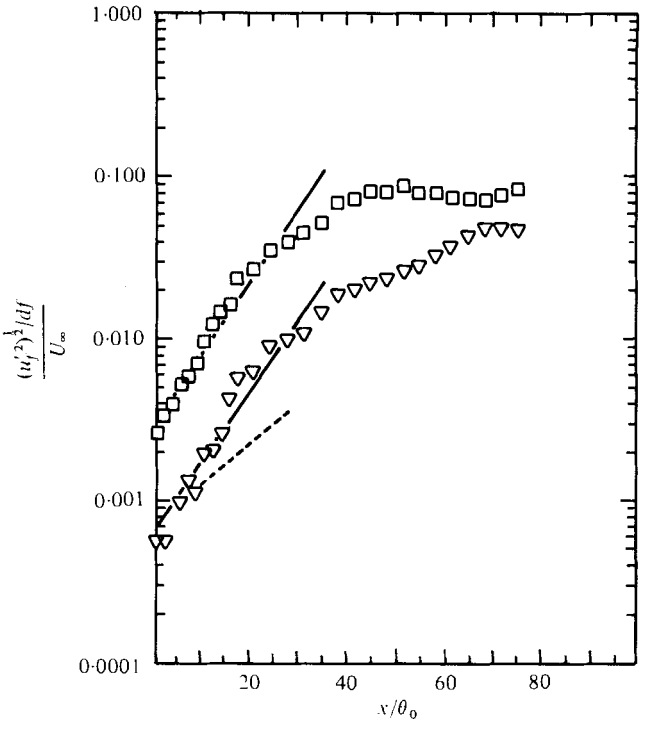

FIGURE 15. Growth rates of $0{\cdot}5\beta_I$ and β_I components with increasing downstream distance; from spectral analysis of hot-film output with probe at location of maximum fluctuating amplitude. $R_{\theta_0} = 190$, $L/\theta_0 = 80$. $0{\cdot}5\beta$-component: ∇, data; – – – –, theory. β-component: $\square$, data; ——, theory.

over, in accordance with the measurements of Freymuth (1966), who showed that decreasing the amplitude of external excitation of a non-impinging jet increases the streamwise extent of the linear-growth region, the weaker value of fluctuation amplitude of the fundamental (β_{II}) at $x = 0^+$ results in a longer linear region (figures 16, 17) than that resulting from the initially stronger value of the fundamental (β_I) component (figures 14, 15).

To provide further insight into the self-sustaining amplitude-modulation process, streamwise variation of phase is required; for the nonlinear coupling criterion for wavenumbers to be satisfied, as was previously assumed, all components must have the same phase speed. In § 7, attention is given to the near-field phase distributions of each of the components of the self-modulated impinging flow, as well as the overall phase difference between separation and impingement.

7. Overall phase conditions for fundamental and low-frequency components

Cross-spectral analysis of the velocity signal from the hot-film probe located at the edge of the shear layer and the fixed pressure probe was carried out to evaluate the streamwise phase distributions at each of the discrete frequency components. The same two characteristic lengths, $L/\theta_0 = 80$ and 100, used in the previous experiments, were again employed.

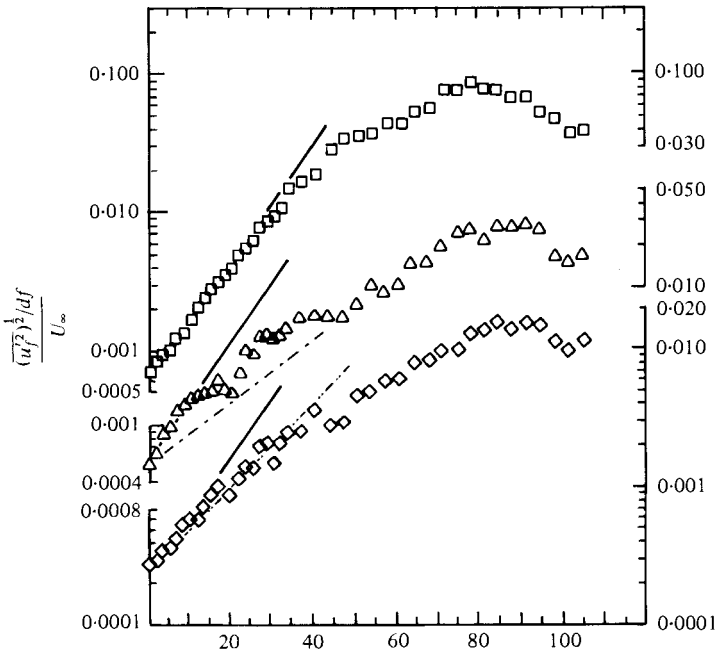

FIGURE 16. Growth rates of $0{\cdot}4\beta_{II}$, $0{\cdot}6\beta_{II}$, and β_{II} components with increasing downstream distance; from spectral analysis of hot-film output with probe located at y-location corresponding to $u/U = 0{\cdot}95$. $R_{\theta_0} = 190$, $L/\theta_0 = 100$. $0{\cdot}4\beta$-component: △, data; — — —, theory. $0{\cdot}6\beta$-component: ◇, data; — — — —, theory. β-component: □, data; ——, theory.

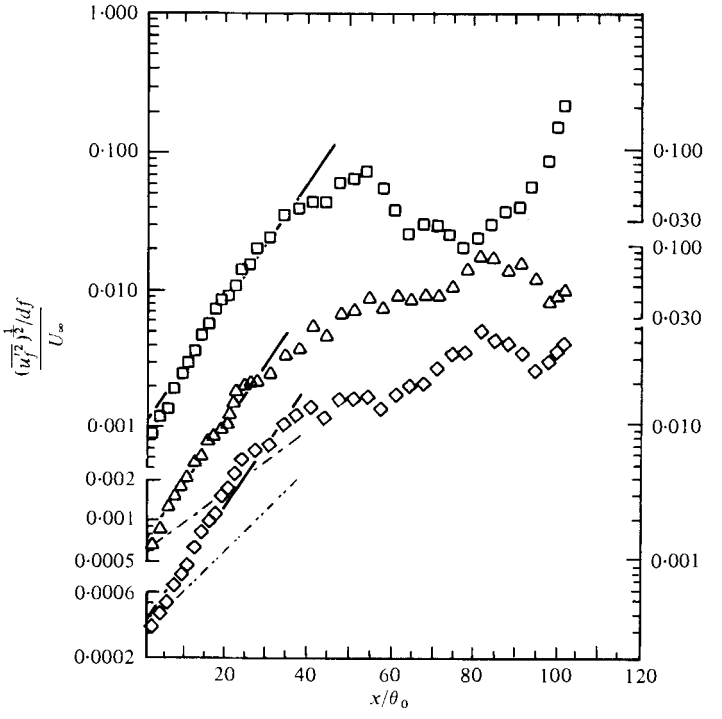

FIGURE 17. Growth rates of $0{\cdot}4\beta_{II}$, $0{\cdot}6\beta_{II}$, β_{II} components with increasing downstream distance; from spectral analysis of hot-film output with probe at location of maximum fluctuating amplitude. $R_{\theta_0} = 190$, $L/\theta_\theta = 100$. Symbols as in figure 16.

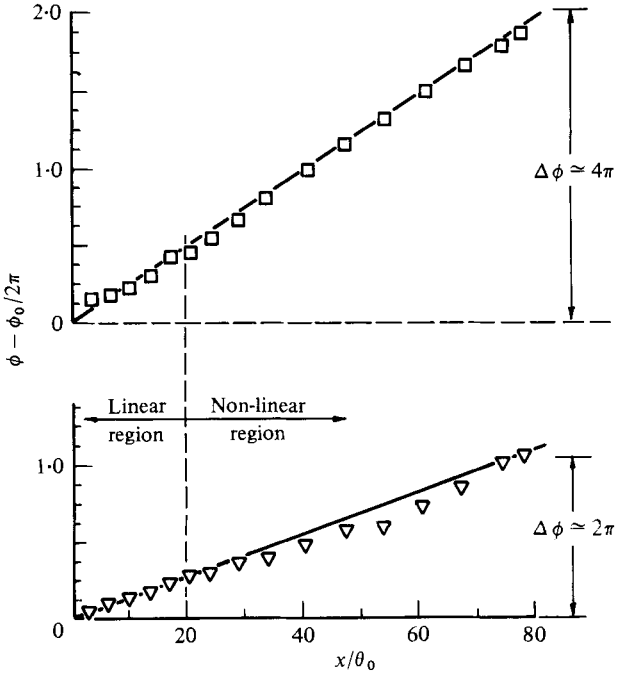

FIGURE 18. Phase variation of $0{\cdot}5\beta_1$ and β_1 components with downstream distance; hot-film probe located at positions where $u/U = 0{\cdot}95$. $R_{\theta_0} = 190$, $L/\theta_0 = 80$. ∇, $0{\cdot}5\beta$-component; $\square$, β.

In figures 18 and 19, the phase of the fundamental frequency component β is seen to vary linearly with downstream distance for both stages of oscillation. Corresponding wavenumbers $2\pi\theta_m/\lambda$ calculated from these phase variations increase with increasing frequency, as predicted by Michalke (1965) (recall that θ_m is a reference momentum thickness near the centre of the linear growth region where $x/\theta_0 = 10$); they are approximately 10–15 % higher than the theoretical values.

The curve through the data for the fundamental is a least-squares, straight-line fit to the experimental data in both figures 18 and 19. To examine the possibility that the low-frequency modulating components and the respective fundamental component travel at the same phase speeds, the required $d\phi/dx$ to effect equal phase speeds was calculated. Knowing the subharmonic frequencies (f_{β_i}), the local phase speeds are given by $c_{\beta_i} = 2\pi f_{\beta_i}(d\phi/dx)^{-1}$. The results of such calculations are lines passing through the subharmonic data. Throughout the shear layer, but especially in the linear region, where all frequency components grow at the rate of the fundamental (see figures 14, 16), the data are well-represented (within experimental accuracy) by the calculated lines. Thus it is concluded that the fundamental and subharmonic component(s) propagate with approximately the same phase speed, which is about $0{\cdot}48U$.

It is noted that all frequency components in figures 18 and 19 appear to undergo a change in phase from separation to impingement (along the edge of the shear layer) that is approximately an integral multiple of 2π. That is, *each low-frequency component independently satisfies the criterion that* $L = k\lambda$, *where* k *is an integer*. This contrasts with the investigation of Sarohia (1975) for a cavity-type flow; in his case, where measurements were taken *within* the shear layer, the relation $L/\lambda \simeq n + \frac{1}{2}$ was found

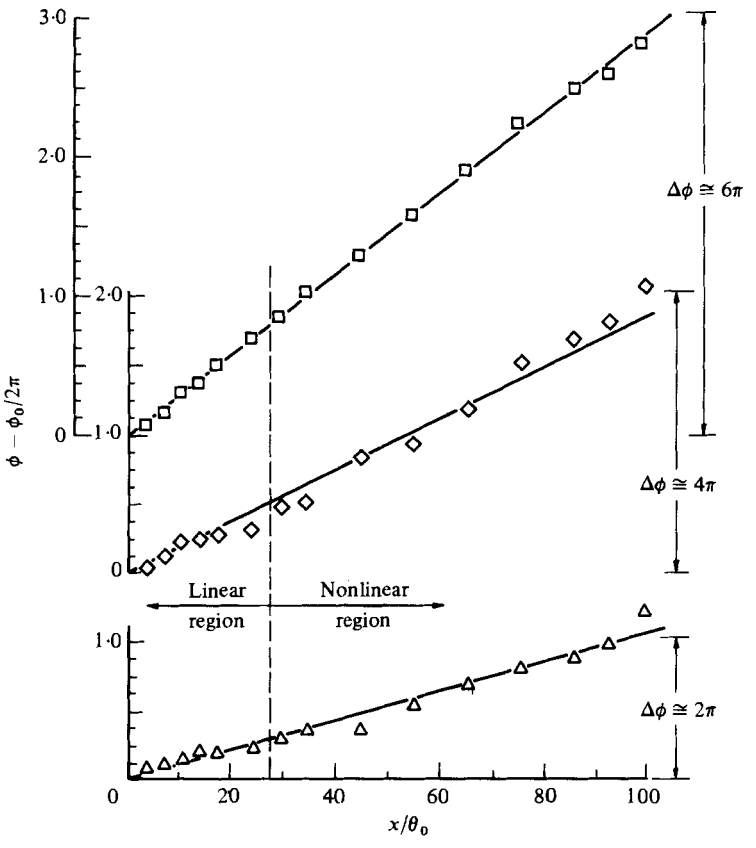

FIGURE 19. Phase variation of $0{\cdot}4\beta_{II}$, $0{\cdot}6\beta_{II}$ and β_{II} components with downstream distance; hot-film probe located at positions where $u/U = 0{\cdot}95$. $R_{\theta_0} = 190$, $L/\theta_0 = 100$. △, $0{\cdot}4\beta$-component; ◇, $0{\cdot}6\beta$; □, β.

to be well-approximated along the mouth ($y = 0$) of the cavity. However, due to the severe phase distortions that Sarohia found to occur near $y = 0$, it seems that the most appropriate location for characterizing the overall phase difference is along the line $u/U = 0{\cdot}95$, i.e. along the edge of the shear layer. Indeed, if one examines Sarohia's phase data along the line $u/U = 0{\cdot}95$, it is seen that the relation $L = k\lambda$ is satisfied.

For the two stages of oscillation examined here, it appears that the number of possible subharmonics is governed by the streamwise phase criterion,

$$\Delta\phi_{\tilde{u}} = \phi_{\tilde{u}_L} - \phi_{\tilde{u}_0} = 2k\pi,$$

where $\phi_{\tilde{u}_L}$ is the phase at impingement and $\phi_{\tilde{u}_0}$ is the phase at separation (both measured at the edge of the shear layer). For stage I, the fundamental has a phase change of 4π from separation to impingement, permitting only one subharmonic with a phase change of 2π. For stage II, the fundamental has a phase change of 6π, which allows for subharmonics with phase changes of 4π and 2π. *In general, for the predominant and persistent oscillation components* (β, $0{\cdot}4\beta$, $0{\cdot}5\beta$, $0{\cdot}6\beta$), *if the fundamental* (β) *satisfies the phase criterion* $\Delta\phi = 2k\pi$, *it is expected that* $k-1$ *subharmonics may be present* with overall phase differences of $2(k-1)\pi, 2(k-2)\pi, \ldots, 2\pi$; *the lowest admissible subharmonic having an overall phase difference of* 2π.

8. Conclusions

This experimental investigation of low-frequency self-modulation of an impinging cavity shear layer indicates that the low-frequency components are associated with the interaction of successive shear-layer vortices with the downstream cavity corner. This cyclic transverse displacement of the shear layer at impingement is interpreted as a low-frequency flapping of the shear layer. Low-frequency components were found to persist over a twofold range of both mean velocity and impingement length. Two distinct stages of oscillation were observed, one with a single subharmonic (stage I) and one with dual subharmonics (stage II). Detailed study of two representative lengths, one from each of these stages, indicated that the low-frequency flapping motion has a wavelength equal to the cavity length and interacts nonlinearly with the shear-layer instability. This interaction can be written in the form

$$\cos[2\pi(\alpha\beta)t+\phi_{\alpha\beta}]\cos[2\pi\beta t+\phi_{\beta}],$$

indicating an amplitude-modulated process. A trigonometric identity allows this modulation to be written as sum, $(1+\alpha)\beta$, and difference, $(1-\alpha)\beta$, frequencies. The nonlinear generation of the difference frequency was found to be the stronger of the two, as we also found for dual-frequency external excitation of both a turbulent jet (Ronneberger & Ackermann 1979) and a non-impinging shear layer (Miksad 1973).

The authors gratefully acknowledge the financial support of the National Science Foundation, Washington, D.C., at the Volkswagen Foundation, Hannover, West Germany, during the course of this investigation.

REFERENCES

BLACKMAN, R. B. & TUKEY, J. W. 1958 *The Measurement of Power Spectra.* Dover.

BREIDENTHAL, R. 1979 Chemically reacting, turbulent shear layer. *A.I.A.A. J.* **17**, 310–311.

BRILLINGER, D. R. & ROSENBLATT, M. 1967 Computation and interpretation of k-th order spectra. In *Spectral Analysis of Time Series* (ed. B. Harris), pp. 189–232. Wiley.

BROWAND, F. K. 1966 An experimental investigation of the instability of an incompressible, separated shear layer. *J. Fluid Mech.* **26**, 281–307.

BROWAND, F. K. & WEIDMAN, P. D. 1976 Large scales in the developing mixing layer. *J. Fluid Mech.* **76**, 127–144.

CONLISK, A. T. & ROCKWELL, D. O. 1982 Modelling of vortex–corner interaction using point vortices. Submitted for publication.

FFOWCS WILLIAMS, J. E. 1969 Hydrodynamic noise. *Ann. Rev. Fluid Mech.* **1**, 197–222.

FREYMUTH, P. 1966 On transition in a separated laminar boundary layer. *J. Fluid Mech.* **25**, 683–704.

HASSELMANN, K., MUNK, W. H. & MACDONALD, G. J. F. 1963 Bispectra of ocean waves. In *Time Series Analysis* (ed. M. Rosenblatt), pp. 125–139. Wiley.

HAUBRICH, R. 1965 Earth noise, 5 to 500 millicycles per second. *J. Geophys. Res.* **70**, 1415–1427.

HUSSAIN, A. K. M. F. & ZAMAN, K. B. M. Q. 1978 The free shear layer tone phenomenon and probe interference. *J. Fluid Mech.* **87**, 349–383.

KELLY, R. E. 1967 On the stability of an inviscid shear layer which is periodic in space and time. *J. Fluid Mech.* **27**, 657–689.

KIM, Y. C. & POWERS, E. J. 1978 Digital bispectral analysis of self-excited fluctuation spectra. *Phys. Fluids* **21**, 1452–1453.

KIM, Y. C. & POWERS, E. J. 1979 Digital bispectral analysis and its application to nonlinear wave interactions. *I.E.E.E. Trans. Plasma Sci.* PS-**7**, 120–131.

KIM, Y. C., BEALL, J. M., POWERS, E. J. & MIKSAD, R. W. 1980 Bispectrum and nonlinear wave coupling. *Phys. Fluids* **23**, 258–263.

KNISELY, C. W. 1980 An experimental investigation of low frequency self-modulation of incompressible impinging cavity shear layers. Ph.D. dissertation, Lehigh University, Bethlehem, Pa.

KONRAD, J. H. 1976 An experimental investigation of mixing in two-dimensional turbulent shear flows with applications to diffusion-limited chemical reactions. *Project SQUID Tech. Rep.*, no. CIT-8-PU.

LAU, J. C., FISHER, M. J. & FUCHS, H. V. 1972 The intrinsic structure of turbulent jets. *J. Sound Vib.* **22**, 379–406.

LII, K. S., ROSENBLATT, M. & VAN ATTA, C. 1976 Bispectral measurements in turbulence. *J. Fluid Mech.* **77**, 45–62.

MAULL, D. J. & EAST, L. F. 1963 Three-dimensional flows in cavities. *J. Fluid Mech.* **16**, 620–632.

MICHALKE, A. 1965 On spatially growing disturbances in an inviscid shear layer. *J. Fluid Mech.* **23**, 521–544.

MIKSAD, R. W. 1972 Experiments on the nonlinear stages of free-shear-layer transition. *J. Fluid Mech.* **56**, 695–719.

MIKSAD, R. W. 1973 Experiments on nonlinear interactions in the transition of a free shear layer. *J. Fluid Mech.* **59**, 1–21.

MORKOVIN, M. V. & PARANJAPE, S. V. 1971 On acoustic excitation of shear layers. *Z. Flugwiss.* **19**, 328–335.

POWELL, A. 1961 On the edgetone. *J. Acoust. Soc. Am.* **33**, 395–409.

ROCKWELL, D. & KNISELY, C. 1979*a* The organized nature of flow impingement upon a corner. *J. Fluid Mech.* **93**, 413–432.

ROCKWELL, D. & KNISELY, C. 1979*b* Unsteady features of flow past a cavity. *J. Hydraul. Div. A.S.C.E.* **105**, 969–979.

ROCKWELL, D. & KNISELY, C. 1980*a* Observations of the three-dimensional nature of unstable flow past a cavity. *Phys. Fluids* **23**, 425–431.

ROCKWELL, D. & KNISELY, C. 1980*b* Vortex–edge interaction: mechanisms for generating low frequency components. *Phys. Fluids* **23**, 239–240.

ROCKWELL, D. & NAUDASCHER, E. 1979 Self-sustained oscillations of impinging free shear layers. *Ann. Rev. Fluid Mech.* **11**, 67–94.

RONNEBERGER, D. & ACKERMANN, U. 1979 Experiments on sound radiation due to nonlinear interaction of instability waves in a turbulent jet. *J. Sound Vib.* **62**, 121–129.

ROSENBLATT, M. & VAN NESS, J. W. 1965 Estimation of the bispectrum. *Ann. Math. Stat.* **36**, 1120–1136.

SAROHIA, V. 1975 Experimental and analytical investigation of oscillations in flows over cavities. Ph.D. dissertation, Cal. Inst. Tech.

SATO, H. 1971 An experimental study of nonlinear interaction of velocity fluctuations in the transition region of a two-dimensional wake. *J. Fluid Mech.* **44**, 741–756.

STEGEN, G. R. & KARAMCHETI, K. 1970 Multiple tone operation of edge tones. *J. Sound Vib.* **12**, 281–284.

STUART, J. T. 1967 On finite amplitude oscillations in laminar mixing layers. *J. Fluid Mech.* **29**, 417–440.

WINANT, C. D. & BROWAND, F. K. 1974 Vortex pairing: the mechanism of turbulent mixing-layer growth at moderate Reynolds number. *J. Fluid Mech.* **63**, 237–255.

ZIADA, S. & ROCKWELL, D. 1982 Oscillations due to an unstable mixing layer impinging upon an edge. Submitted to *J. Fluid Mech.*